Nonlinear characteristics of damaged bridges under moving loads using parameter optimization variational mode decomposition

Jiantao Li[1], Jian Guo[1,2*], Xinqun Zhu[3], Yang Yu[4]

[1]College of Civil Engineering, Zhejiang University of Technology, Zhejiang, China

[2]School of Civil Engineering, Southwest Jiaotong University, Chengdu, China

[3]School of Civil and Environmental Engineering, University of Technology Sydney, NSW, Australia

[4]Centre for Infrastructure Engineering, School of Engineering, Design and Built Environment, Western Sydney University, NSW, Australia

*Correspondence: Jian Guo, School of Civil Engineering, Southwest Jiaotong University, Chengdu 610031, China.

Email: Guoj@Vip.163.com

Abstract

Investigation on the dynamic characteristics of bridges for structural condition assessment is challenging when nonlinear breathing cracks in the bridge and nonstationary vehicle-bridge interaction are considered. Variational mode decomposition (VMD) method has been widely used to analyze the nonlinear time-series, but its performance is highly dependent on the parameter setting, i.e., the number of modes and the penalty factor. A new method based on the parameter optimization VMD is proposed to extract the nonlinear dynamic characteristics from responses of bridge under moving vehicle loads in this paper. The Chicken Swarm Optimization (CSO) algorithm is used to optimize the VMD parameters to improve the decomposition and characterization. A general breathing crack model is introduced to simulate the bridge damage. The acceleration response of bridge considering the cracks is decomposed by the proposed method. The instantaneous frequency (IF) is then obtained from the time-frequency representation (TFR) of the bridge-related response component using the ridge detection. Numerical simulations are performed to investigate the effect of the crack location and extent on the IFs for structural damage detection. The effect of the vehicle-bridge interaction is also discussed. The method is further verified using the laboratory experimental results of a concrete bridge model under the vehicle load. The nonstationary and nonlinear dynamic properties of the bridge model with different damage scenarios are successfully identified. The results show that the extracted IF clearly reveals the behaviour of breathing crack that can be a potential indicator of the damage in the bridge.

Keywords: nonlinear characteristics, breathing crack, instantaneous frequency, VMD, CSO

1. Introduction

Dynamic characterization of the bridge under operational vehicle loads plays a vital role in bridge structural health monitoring for performance evaluation and damage detection [1,2]. Due to the wide application of highway bridges, the study on their dynamic characteristics under the vehicle loads has attracted great attentions of researchers in solving the vehicle-bridge-interaction (VBI) related problems [3,4]. The presence of a heavy traveling vehicle on the bridge may result in the nonstationary dynamic characteristics of the VBI system causing variations of the structural modal parameters [5]. Moreover, the inevitable cracks emerged in the bridge can lead to the complex nonstationary and nonlinear characteristics in structural dynamic behaviour when the vehicle is moving over the bridge [6, 7]. The studies have shown that the nonlinear dynamic characteristics of structures are sensitive to the breathing crack [8]. A crack on the bridge will open and close during its vibration under operational vehicle loads. The edges of the crack come into and out of contact leading to changes in the dynamic properties of the structure which is known as the breathing process

of the crack [9]. The nonlinear characteristics of the structure can be a good damage indicator, especially the breathing crack damage [10]. Therefore, it is essential to investigate these nonlinear dynamic characteristics for bridge condition assessment.

The nonlinear effects caused by a breathing crack in the structural element have been reported in numerous works. Bovsunovsky and Surace [11] presented a state-of-the-art review to illustrate the nonlinear effects caused by a breathing crack. While the studies of nonlinear behaviour at free and resonant vibrations of beams [9, 12] or when beam is subjected to moving masses [13, 14] are extensive, studies that deal with the nonstationary and nonlinear VBI problems under the effect of breathing cracks are relatively less reported. Law and Zhu [15] proposed to use a crack model as presented in [16] to express the degradation in the flexural rigidity to study the dynamic responses of a cracked bridge. The opening/closing behaviour was modelled by multiplying a time dependent parameter to the degradation damage variable [17]. Nguyen [18] compared the open and breathing crack detection of a beam-like bridge by analyzing the displacement response of the bridge under a moving vehicle. Yin et al. [19] studied the dynamic behaviour of a bridge with multi-cracks under moving vehicles. The massless rotational spring was adopted to describe the local flexibility induced by a crack on the bridge. From the above studies, it is observed that the presence of crack results in high deflections and alters beam response patterns. Moreover, to appropriately model the crack influence on the stiffness of mechanical systems, the most common way was to use a cracked element with additional compliance determined using the energy release rate method based on the fracture mechanics [11, 20].

Some experiential studies have been conducted to explore the nonstationary vibrations of the bridge under moving vehicles. Pakrashi et al. [21] presented an experimental study on the evolution of a crack in a phenolic beam using beam-vehicle interaction responses. An open crack model was introduced by notching in the lower section of the beam. McGetrick [22] constructed a scaled vehicle-bridge interaction model in the laboratory. Damage was simulated via rectangular saw-cuts in the flanges of the steel I-beam. The bridge was modelled as a steel beam with rectangular cross-section and the local damage was simulated as the additional mass put on the beam [23]. Cantero et al. [24] explored the bridge frequency evolution during the passage of vehicles using a scaled laboratory model, where an I-section steel beam was adopted. Some field VBI experimental tests were also conducted for the bridge modal identification and condition inspection [25, 26]. However, these experimental investigations did not consider the nonlinear effects due to breathing cracks.

A key feature of the nonlinear behaviour of cracked bridge subjected to moving vehicle load is an instantaneous change of the bridge stiffness at crack opening and closing. To characterize the nonlinear behaviour of a bridge subjected to moving vehicle loads, a variety of methods have been developed to examine the instantaneous frequency (IF) of the bridge under moving loads. Wavelet analysis [18] and empirical mode decomposition (EMD) [27] were used to analyze the non-stationary dynamic responses of vehicle-bridge interaction dynamic system, as well as the improved empirical wavelet transform [28] and modified S-transform reassignment [29]. Due to the solid mathematical theoretical foundation compared to the abovementioned methods, variational mode decomposition (VMD) methods have been proved to be effective in analyzing the nonstationary and nonlinear dynamic responses [30,31]. The efficacy and accuracy of VMD based method compared to EMD have been demonstrated in [32,33]. Despite of its wide applications, the performance of VMD heavily depends on the proper parameter setting, i.e., the number of modes and the quadratic penalty factor. Some attempts have been made to optimize the parameters using different optimization algorithms, such as the particle swarm optimization (PSO) [34]. The chicken swarm optimization (CSO) algorithm can be used to solve the optimization effectively in terms of optimization accuracy,

robustness and conciseness [35]. It has been confirmed that CSO outperforms many nature-inspired algorithms like PSO and genetic algorithm in solving a wide range of standard benchmark and real-life problems [36,37]. Therefore, a novel improved VMD method with parameter-optimized by CSO (CSO-VMD) is proposed to study the nonlinear dynamic characteristics of cracked bridges.

The objective of this study is to identify the nonlinear characteristics of the cracked bridge under moving vehicle loads. A cracked finite element is developed by considering an overall additional flexibility to the flexibility matrix of intact element [38] based on the fracture mechanics. The breathing crack switching between being open and closed states is considered according to the curvature at the crack location. A novel CSO-VMD method integrated with ridge detection technique is proposed for IF identification of the nonlinear and/or nonstationary bridge response of the VBI system. The identified IFs are analyzed for possible crack detection. Moreover, the experimental study of a VBI model is conducted in the laboratory where the crack damages are introduced to the concrete bridge model. It is not only to validate the proposed analytical method, but also to provide information of practical engineering relevance for analyzing the structural nonlinear properties under a moving vehicle. The rest of paper is organized as followings: Section 2 introduces a generic bridge model under moving loads considering the nonlinear dynamic behaviour due to the breathing cracks; Section 3 presents the algorithm for the nonlinear characteristic identification of the bridge; Section 4 conducts the numerical analysis to demonstrate the effectiveness of the proposed method in revealing the nonlinear characteristics of bridge and localizing the cracks. The implementation of an experimental verification on nonlinear characteristics of a typical Tee-beam under the model vehicle load is discussed in Section 5. Finally, the conclusions are drawn in Section 6.

2. Numerical modelling of a cracked bridge subjected to moving loads

2.1 Bridge model subjected to moving loads

The governing equation of motion of a damped beam bridge with NN degrees-of-freedom (DOFs) subjected to moving vehicle loads can be expressed as

$$\mathbf{M}_b \ddot{\mathbf{x}}_b + \mathbf{C}_b \dot{\mathbf{x}}_b + \mathbf{K}_b \mathbf{x}_b = \mathbf{\Phi} \mathbf{P}(t) \tag{1}$$

where $\mathbf{M}_b$, $\mathbf{C}_b$ and $\mathbf{K}_b$ are the $NN \times NN$ mass, damping and stiffness matrices of the bridge, respectively; $\mathbf{P}(t)$ are the moving loads on the bridge; $\mathbf{\Phi}$ is the Hermitian cubic interpolation functions for transforming the moving loads $\mathbf{P}(t)$ to equivalent nodal forces to the beam element of the bridge [19].

2.2 Bridge cracked element models

The local structural damage of the bridge is usually considered as the reduction of flexural stiffness. An overall flexibility matrix is especially appropriate for the analysis of a cracked beam based on a fracture mechanics approach considering the relationship between the strain energy release rate and the stress intensity factor [11]. A description for deriving the stiffness matrix of an open cracked element is presented as below.

2.2.1 Stiffness matrix of an open cracked element

For a rectangular cross-sectional beam element with height h, width b and length L_e, the additional strain energy due to the existence of the crack considering only the bending deformation can be expressed as [38]

$$\Pi_c = b \int_0^a W \, da = b \int_0^a \frac{(K_{I2} + K_{I3})^2 + K_{II2}{}^2}{E'} \, da \tag{2}$$

where Π_c is the additional strain energy due to the crack; a is the total depth of the crack; W is the strain energy release rate function; $E' = E$ is the Young's modulus for plane stress problem and

$E' = E/(1 - \mu^2)$ for plane strain problem; μ is Poisson's ratio; K_{I2}, K_{II2} and K_{I3} are the stress intensity factors due to shear force V and bending moment M at the right node of the element, respectively; $K_{I2} = \frac{6VL_c}{bh^2}\sqrt{\pi a}F_2(\frac{a}{h})$; $K_{I3} = \frac{6M}{bh^2}\sqrt{\pi a}F_2(\frac{a}{h})$, in which F_2 and F_{II} are the correction factors for stress intensity factors. They can be expressed as

$$F_2(s) = \sqrt{\frac{\text{tg}(\pi s/2)}{\pi s/2}}\frac{0.923 + 0.199(1 - \sin(\pi s/2))^4}{\cos(\pi s/2)} \quad (s = \frac{a}{h}) \tag{3}$$

$$F_{II}(s) = \frac{1.122 - 0.561s + 0.085s^2 + 0.180s^3}{\sqrt{1-s}} \quad (s = \frac{a}{h}) \tag{4}$$

Using Paris equation, the entries of the overall additional flexibility matrix c_{ij} can be expressed as

$$c_{ij} = \frac{\partial^2 \Pi_c}{\partial P_i \partial P_j}, \quad i,j = 1,2; \tag{5}$$

$$c_{ij} = \frac{b}{E'}\frac{\partial^2}{\partial P_i \partial P_j}\int_0^a \left\{\left[\frac{6VL_c}{bh^2}\sqrt{\pi\xi}F_2\left(\frac{\xi}{h}\right) + \frac{6M}{bh^2}\sqrt{\pi\xi}F_2\left(\frac{\xi}{h}\right)\right]^2 + \left[\frac{V}{bh}\sqrt{\pi\xi}F_{II}\left(\frac{\xi}{h}\right)\right]^2\right\} d\xi \tag{6}$$

The dimensionless forms can be expressed as follows (by setting $x = a/h$):

$$F(1,1) = c_{11}E'b = 2\pi\left[\frac{36L_c^2}{h^2}\int_0^{a/h}xF_2^2(x)\,dx + \int_0^{a/h}xF_{II}^2(x)\,dx\right] \tag{7}$$

$$F(1,2) = \frac{c_{12}E'bh^2}{L_c} = 72\pi\int_0^{a/h}xF_2^2(x)\,dx \tag{8}$$

and, $F(2,2) = c_{22}E'bh^2 = F(1,2)$; $c_{21} = c_{12}$. The entries of the overall additional flexibility matrix c_{ij} can be obtained using least squares best-fitted formulas of $F(1,1)$ and $F(2,2)$.

The overall additional flexibility matrix can be expressed as $C_{ovl} = \begin{bmatrix} c_{11} & c_{12} \\ c_{21} & c_{22} \end{bmatrix}$. The total flexibility matrix of the cracked beam element can now be obtained by

$$C_{tot} = C_{intact} + C_{ovl} = \begin{bmatrix} \frac{L_e^3}{3EI} + c_{11} & \frac{L_e^2}{2EI} + c_{12} \\ \frac{L_e^2}{2EI} + c_{21} & \frac{L_e}{EI} + c_{22} \end{bmatrix} \tag{9}$$

where C_{intact} is the flexibility matrix of the intact beam element. The stiffness matrix of a cracked beam element can be obtained as follows:

$$K_c = LC_{tot}^{-1}L^T \tag{10}$$

where $L = \begin{pmatrix} -1 & -L_e & 1 & 0 \\ 0 & -1 & 0 & 1 \end{pmatrix}^T$.

2.2.2 Stiffness matrix of a breathing cracked element

A breathing cracked element depending on the curvature of the beam at the crack location is use to build the stiffness matrix [14,18]. The stiffness can be expressed as a continuous function as follows.

$$K_b = K_e + 1/2(K_c - K_e)\left[1 + \frac{d''}{d''_{max}}\right] \tag{11}$$

where K_b is the stiffness of the element with a breathing crack; K_e is the stiffness of the intact element; d'' is the instantaneous curvature of the beam at the crack position and d''_{max} is the maximum curvature of the beam at the crack position with the passage of the vehicle load. The equation shows that when $d'' = d''_{max}$ the stiffness K_b is minimum and equal to the stiffness of an

4

open cracked element K_c. By this method, the stiffness of a breathing cracked element can be determined based on the stiffness of an open cracked and intact element.

The beam curvature $d''(x)$ is approximated by the second derivative of the deflection that can be calculated with the nodal displacements and rotations of the beam element. It is important to note that the d''_{max} depends on the properties of the moving load such that it cannot be set a *priori*. Since the maximum value of the curvature is unknown, it is initially obtained from a fully open crack problem. Having known the maximum curvature at crack location, the matrix K_b is then calculated at each instant of time. The deflections of all nodal points are determined by solving the system of differential equations using Newmark-beta method. This process continues till the moving loads reach to the end of the beam. The maximum curvature at crack location is recorded during the moving load excitation. The problem solves again with this new maximum curvature. This loop continues until the difference between the two last maximum curvatures becomes less than a given tolerance value.

2.2.3 The global stiffness matrix of the cracked bridge

The global stiffness matrix of the cracked bridge can be formed by assembling the stiffness matrices of common intact beam elements and the cracked elements. The stiffness matrix of the common intact beam element K_e can be derived as:

$$K_e = \frac{EI}{L_e^3}\begin{bmatrix} 12 & 6L_e & -12 & 6L_e \\ 6L_e & 4L_e^2 & -6L_e & 2L_e^2 \\ -12 & -6L_e & 12 & -6L_e \\ 6L_e & 2L_e^2 & -6L_e & 4L_e^2 \end{bmatrix} \tag{12}$$

The global matrix of all the common beam elements $\mathbf{K}_{com}$ can be assembled according to the DOFs of each element with K_e. The entries corresponding to the DOFs of cracked elements in $\mathbf{K}_{com}$ are zeros. Assuming that the number of cracked beam elements is N_c, the global stiffness of the bridge $\mathbf{K}_b$ can be written as

$$[\mathbf{K}_b]_{NN \times NN} = [\mathbf{K}_{com}]_{NN \times NN} + \left[\sum_{i=1}^{N_c} \mathbf{A}_{mi}^T K_{bi} \mathbf{A}_{mi}\right]_{NN \times NN} \tag{13}$$

with

$$\mathbf{A}_{mi} = \begin{bmatrix} 0 & \cdots & 0 & 1 & 0 & 0 & 0 & 0 & 0 & 0 & \cdots & 0 \\ 0 & \cdots & 0 & 0 & 1 & 0 & 0 & 0 & 0 & 0 & \cdots & 0 \\ 0 & \cdots & 0 & 0 & 0 & 1 & 0 & 0 & 0 & 0 & \cdots & 0 \\ 0 & \cdots & 0 & 0 & 0 & 0 & 1 & 0 & 0 & 0 & \cdots & 0 \end{bmatrix}_{4 \times NN} \tag{14}$$

where, K_{bi} and mi are the stiffness matrix and the serial number of the i-th cracked element, respectively; $\mathbf{A}_{mi}$ is the transformation matrix of the i-th cracked element that its entries are all zeros expect at its corresponding DOFs.

3. The algorithm for the dynamic characteristic analysis

3.1 Variational mode decomposition

The fundamental of VMD is briefly introduced, while more detailed information can be obtained in [30]. The bridge response $\ddot{x}_b(t)$ can be expressed as a combination of K number of amplitude-modulated and frequency-modulated components with a limited frequency bandwidth [31].

$$\ddot{x}_b(t) = \sum_{i=1}^{K} u_i(t) \tag{15}$$

where K is the number of the components $\{u_i(t), i = 1, 2, \dots K\}$. The VMD can decompose the bridge response into components with an adaptive filter. The decomposition can be considered as a constrained variational problem with the corresponding objective function expressed as

$$f_{\text{obj}} = \min \Sigma_{\{u_i(t)\}\{\overline{\omega}_i\}} \left\{ \Sigma_{i=1}^{K} \left\| \partial_t \left[\left(\delta(t) + \frac{j}{\pi t} \right) * u_i(t) \right] e^{-j\overline{\omega}_i t} \right\|_2^2 \right\} \tag{16}$$

$$\text{subject to} \qquad \ddot{x}_b(t) = \Sigma_{i=1}^{K} u_i(t),$$

where δ is the Dirac function; $*$ is the convolution symbol; $u_i(t)$ and $\overline{\omega}_i$ (for $i=1...K$) represent the different components of the response and their corresponding center frequencies, respectively.

By introducing the quadratic penalty factor α and multiplication operator λ, the optimization objective function of optimization problem in Eq.(16) can be transferred into an unconstrained optimization problem as follows:

$$L(\{u_i(t)\}, \{\overline{\omega}_i\}, \lambda) = \alpha \sum_{i=1}^{K} \left\| \partial_t \left[\left(\delta(t) + \frac{j}{\pi t} \right) * u_i(t) \right] e^{-j\overline{\omega}_i t} \right\|_2^2$$

$$+ \left\| \ddot{x}_b(t) - \Sigma_{i=1}^{K} u_i(t) \right\|_2^2 + \langle \lambda(t), \ddot{x}_b(t) - \Sigma_{i=1}^{K} u_i(t) \rangle \tag{17}$$

Then, the alternate direction method of multipliers approach [31, 40] is used to solve the variational problem in Eq.(17). The complete optimization problem is divided into a sequence of iterative sub-optimization problems.

3.2 Parameter optimization for VMD

It is generally recognized that the component number K and the penalty factor α have a significant impact on the performance of VMD. Finding the optimal values of these two variables are essential. CSO is to be used for searching the optimal values of K and α with a fitness function which is made up of the average of both correlation coefficient and energy loss coefficient [40]. It is described as follows:

$$f_{\text{ACE}}(K, \alpha) = \frac{C+E}{2} \tag{18}$$

where $f_{\text{ACE}}(K, \alpha)$ is the fitness function regarding the parameters of VMD; C indicates the maximum correlation coefficient between all modes, and E denotes the energy loss coefficient.

$$C = \max\left(\{C_i^j\}\right) \tag{19}$$

$$C_i^j = \frac{\Sigma_{t=1}^{N}[u_i(t)-\overline{u}_i][u_j(t)-\overline{u}_j]}{\sqrt{\Sigma_{t=1}^{N}[u_i(t)-\overline{u}_i]^2}\sqrt{\Sigma_{t=1}^{N}[u_j(t)-\overline{u}_j]^2}} \tag{20}$$

where C_i^j is the set of all correlation coefficients in a VMD result; u_i and u_j are two different modes, and $\overline{u}_i$ and $\overline{u}_j$ are the mean of u_i and u_j, respectively. As the energy loss coefficient, E is defined as the ratio of the energy of the decomposition residual to the energy of the original signal, which can be calculated by the following formula:

$$E = \frac{\Sigma_{t=1}^{N}[\ddot{x}_b(t)-\Sigma_{i=1}^{M} u_i(t)]^2}{\Sigma_{t=1}^{N}[\ddot{x}_b(t)]^2} \tag{21}$$

where $\ddot{x}_b(t)$ is the original signal; N is the length of the signal data, and M is the number of modes. Therefore, the parameter optimization of VMD for a signal can be described as follows:

$$\begin{array}{c} \arg f_{\text{ACE}}(K, \alpha) \\ K, \alpha \end{array} = \begin{array}{c} \arg \min \left(\frac{C+E}{2}\right) \\ K, \alpha \end{array} \tag{22}$$

3.3 IF identification based on Chicken Swarm Optimization for VMD

3.3.1 CSO

The chicken swarm optimization algorithm mimics the hierarchal order and behaviors of searching food in the chicken swarm. The whole chicken swarm is divided into three groups of chickens, i.e., rooster, hen, and chick. When the CSO algorithm solves the optimization problem of Eq.(22), each chicken represents a feasible solution and different chickens follow different optimization strategies. In performing CSO algorithm, assume that the total population number of chickens is N, among which there are N_r roosters, N_c chicks, N_h hens, and the number of mother hens is N_m. The chickens are arranged in rising order according to their individual fitness values. The N_r chickens in front with the best fitness are defined as roosters, and the N_c chickens at last with the worst fitness values are called chicks. The remaining N_h $(=N-N_r-N_c)$ chickens in the middle are treated as hens, and the mother hens are randomly selected from the hens. Each virtual chicken is a vector consisting of D elements, where D denotes the dimension of the solution space (control variables), i.e. $D=2$ in this study. Let $x_{i,j}^t$ denotes the position of the i-th chicken in the j-th dimension of solution space in the t-th iteration, where $i \in (1,2,\dots,N), j \in (1,\dots,D), t \in (1,2,\dots,T_{max})$; T_{max} is the maximal iterative number.

The position update formula of different types of chickens in each iteration is as follows [36, 37].
(1) The position updating of rooster is formulated as:

$$x_{i,j}^{t+1} = x_{i,j}^{t,\text{best}} + randn(0,\sigma^2) * x_{i,j}^{t,\text{best}} \tag{23}$$

$$\sigma^2 = \begin{cases} 1, & if\ f_i \leq f_k \\ \exp\left(\frac{f_k-f_i}{|f_i|+\varepsilon}\right), otherwise, \end{cases} \quad i, k \in [1,N], k \neq i \tag{24}$$

where, $x_{i,j}^{t+1}$ is the position of j-th dimension of a chicken i in $t+1$ iteration; $x_{i,j}^{t,\text{best}}$ is the position of the i-th chicken in t-th iteration, which corresponds to the smallest fitness value; $randn(0,\sigma^2)$ is a random number of Gaussian distribution whose variance is σ^2; ε is infinitesimal to avoid zero-division-error; k is a rooster's index, randomly selected from the rooster's group; f_i and f_k are the fitness values of roosters i and k, respectively.
(2) The position updating of hens can be expressed as

$$x_{i,j}^{t+1} = x_{i,j}^{t,\text{best}} + S1 * Rand * \left(x_{r1,j}^t - x_{i,j}^t\right) + S2 * Rand * \left(x_{r2,j}^t - x_{i,j}^t\right) \tag{25}$$

$$S1 = \exp\left((f_i - f_{r1})/(abs(f_i + \varepsilon))\right) \tag{26}$$
$$S2 = \exp\left((f_{r2} - f_i)\right) \tag{27}$$

where $x_{r1,j}^t$ is the position of individual rooster individual $r1$ in the population of hen x_i; $x_{r2,j}^t$ is the position of random individual $r2$ (rooster or hen) in the other population ($r1 \neq r2$), respectively; $Rand$ is a random number in the interval $[0,1]$; $S1$ and $S2$ denote the weights; f_{r1} and f_{r2} are the fitness value of individual rooster in the population of hen x_i and random individual $r2$ in the other population, respectively;
(3) The position updating of chicks can be formulated as:

$$x_{i,j}^{t+1} = x_{i,j}^t + FL * \left(x_{m,j}^t - x_{i,j}^t\right), \ FL \in [0,2] \tag{28}$$

where FL is a parameter, indicating the degree that the chick would follow its mother to forage for food; $x_{m,j}^t$ stands for the position of the mother of i-th chick ($m \in [1, N_m]$)

(4) The change of hierarchical order: the status of the chicken swarm's hierarchical order will remain stable during a period of time. To guarantee the optimal solution, these statuses should be updated every G iterations to adapt to changes in chickens' fitness values.

3.3.2 CSO-VMD

The procedure of CSO-VMD is depicted as follows:

(1) Parameter initialization: the total number of chickens (N), the number of roosters (N_r), hens (N_h), chicks (N_c) and mother hens (N_m), the maximum iterations (T_{max}), the frequency of change of hierarchical order in the swarm (G) are initialized, respectively. The control variables are the positions of the chickens in the CSO algorithm. Their initial values are randomized with the following equation:

$$x_{i.j} = rand * (up_j - low_j) + low_j \qquad (29)$$

where low_j and up_j denote the lower and upper bounds of variable j, respectively.

(2) Generation of hierarchical order in the swarm: the initial hierarchical order is defined according to the fitness values of individual chickens which are calculated by Eq.(22). If the number of iteration time t is divisible by G, the hierarchical order will be updated.

(3) Update the positions and recalculate the fitness values, respectively: roosters, hens, and chicks update their positions according to Eqs.(23), (25), and (28), respectively. Their fitness values are then recalculated using updated positions.

(4) Update individual's best fitness value and the global best fitness value: in this iteration, if the chicken's fitness value is smaller than the previous best one, the chicken's best value and the global best solution will be updated.

(5) Completion of one iteration: if the number of iteration time t is less than T_{max}, return to Step (2). Otherwise, the algorithm is terminated and the global best solution is outputed as the optimal values of control variables, i.e., the optimal values of (K, α) for VMD.

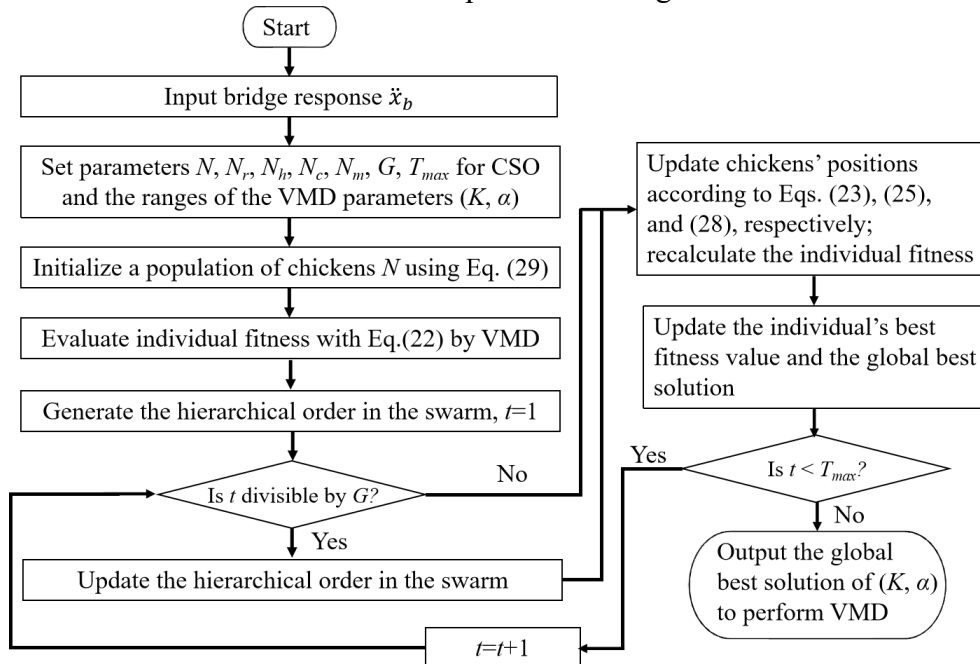The flowchart of the CSO-VMD method is presented in Figure 1.

Figure 1. Flowchart of the proposed CSO-VMD

### 3.3.3 Instantaneous frequency identification

The extraction of the IFs from the decomposed bridge related components can be achieved by Hilbert transform (HT). However, the identified results using HT includes a fast-varying frequency portion that may interfere with the critical nonlinear characteristics due to the crack damage [31,41]. Therefore, ridge detection in TFR of the decomposed component is adopted to estimate the IFs. In this study, the wavelet transform is used to obtain the TFR of the response components extracted by CSO-VMD. The ridge detection approach proposed in [42] is employed to extract the ridge of the TFR that corresponds to the IF at each instant of time.

4. Numerical study

Numerical study is conducted to investigate the dynamic characteristics of the bridge subjected to moving loads. Properties of the target bridge model are: $L = 50m$, $\rho = 7860\,kg/m^3$, $E = 2.1 \times 10^{11} N/m^2$. The Rayleigh damping is considered with the damping ratio being 1%. The breadth and depth of the beam are b=0.5 and a=1.0m, respectively. The first natural frequency of the bridge is 0.94Hz. For structural health monitoring using the nonlinear characteristic of the bridge under a moving vehicle, the vehicle at a low moving speed is recommended [18]. In this study, the vehicle speed is set as 2m/s, unless otherwise specified. The sampling frequency of the numerical simulation is 200Hz.

4.1 Dynamic responses of the bridge under a moving load

The effect of open crack to the bridge is often modelled by a rotational spring connecting two undamaged beam segments considering a crack compliance. To validate the proposed model and algorithm in this study, the mid-span displacement of the bridge under a moving load of 40kN is compared with that by the rotational spring model in [14]. Two crack cases are studied, e.g. the crack depth ratio a/h=0.3 at the location of 1/5L from left support of bridge, and the crack depth ratio a/h=0.4 at mid-span, in correspondence to a moving load at the speed 2m/s and 4m/s, respectively. Figure 2(a) shows the bridge displacement responses at mid-span. The results obtained by the present model are very close to those in [14]. Considering the first crack case, the mid-span acceleration responses of the bridge subjected to a moving load at a speed 2m/s using two crack models are shown in Figure 2(b). In the figure, the results by two models also agree well. The results show that the proposed model is effective and accurate for the crack model.
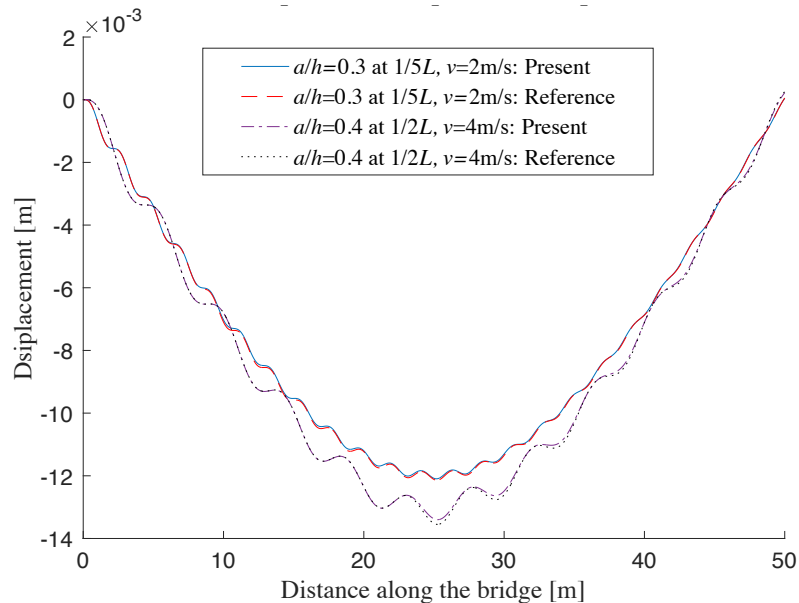
(a) Displacement responses

9
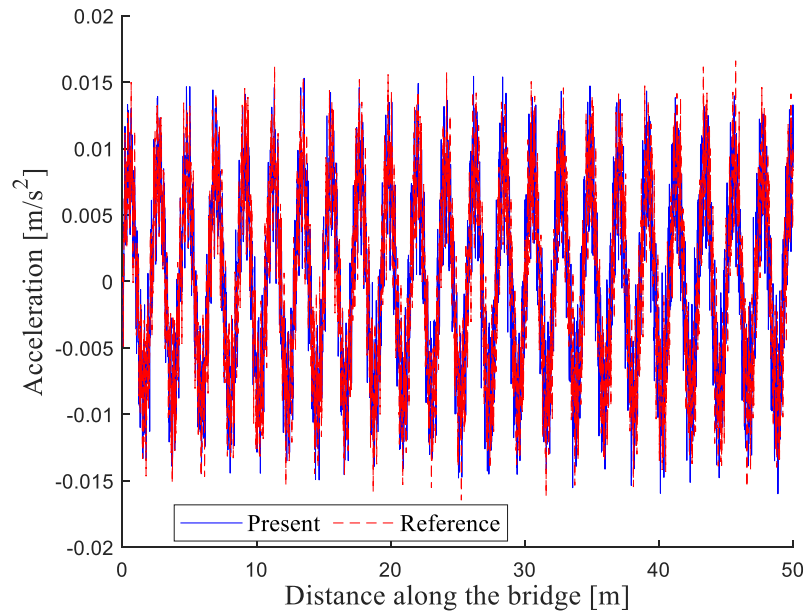
(b) Acceleration responses

Figure 2 Comparison of bridge responses at mid-span subject to a moving load

Figure 3 shows the displacement responses of the bridge at mid-span when the load is passing with a speed of 2m/s considering different crack conditions at mid-span, i.e., no damage, a/h=0.2 and a/h=0.4 for open and breathing crack cases, respectively. The results show that the displacement of the bridge without the crack is much smaller than that with the crack. The displacement response of bridge with a breathing crack is smaller than that with a fully open crack of the same depth, but the difference is not obvious when the crack depth is small, i.e., a/h=0.2. It means that when the crack is small, the behaviors of breathing and open cracks are quite similar and it is difficult to see the opening and closing phenomena of the breathing crack.
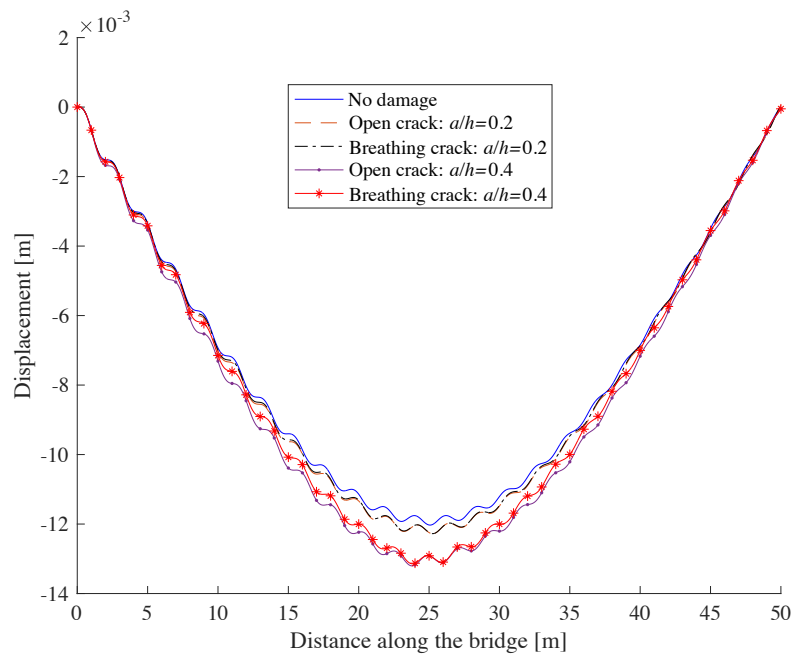
Figure 3 Bridge displacement response at mid-span considering different crack conditions

4.2 Sub- and super-harmonic resonances of a cracked beam

The non-linear dynamic behaviour of a cracked beam due to the crack opening and closing may lead to the manifestation of nonlinear effects such as the sub- and super-harmonic resonances [43]. Thus, the spectral analysis of the vibration response around non-linear resonances has been used for damage detection. The existing study indicates that when the cracked beam is excited by the forcing frequency $f_w = 1/n \cdot f_{b1}$ or $n \cdot f_{b1}$ (n=1, 2, 3,...; f_{b1} is the first bridge natural frequency), the nonlinear behaviour presented in bridge response spectrum can be more visible than that by other exciting frequencies [44, 45]. Therefore, a moving sinusoidal force with its amplitude 10 N and its frequency $f_w = 1/2\, f_{b1}$ is simulated in the same way as [46], which is used to excite the bridge. The exciting force is moving over the bridge at a speed of 2m/s, that the acceleration response measured at 3/8 span of the bridge is used for spectral analysis. The Fourier spectra of bridge responses considering different crack cases of bridge are shown in Figure (4a), with crack depth ratio $a/h=0.4$ at mid-span. For no damage and open crack cases, the principal harmonic component around the exciting frequency f_w has the largest amplitude. The amplitude of the harmonic component around the bridge natural frequency f_{b1} is relative small. For the breathing crack case, the amplitude of the harmonic component around the natural frequency is slightly larger than that around the exciting frequency. Moreover, the response spectrum of the bridge with breathing crack exhibits richer harmonic contents than that of no damage and open crack cases. There are two more harmonics with frequencies approximates to $f_w + f_{b1}$ and $2f_w + f_{b1}$, respectively. The finding is consistent with the results of [44]. Similarly, for the exciting force with frequency $f_w = 2\, f_{b1}$, some sub-harmonic resonances are observed in the response as shown in Figure (4b) for breathing crack case that their frequencies are $3f_w$ and $4f_w$, respectively. The amplitudes of the non-linear resonances are much less significant, i.e. less than 3.2% of the principal resonances. The appearance of the sub-harmonic resonance indicates the presence of the breathing crack. However, using these nonlinear vibration characteristics for structural damage detection has certain drawbacks such as the problems of unstable solutions and pseudo-superharmonic resonances [11]. Therefore, the CSO-VMD based method is developed to increase the sensitivity and reliability of non-linear vibration.
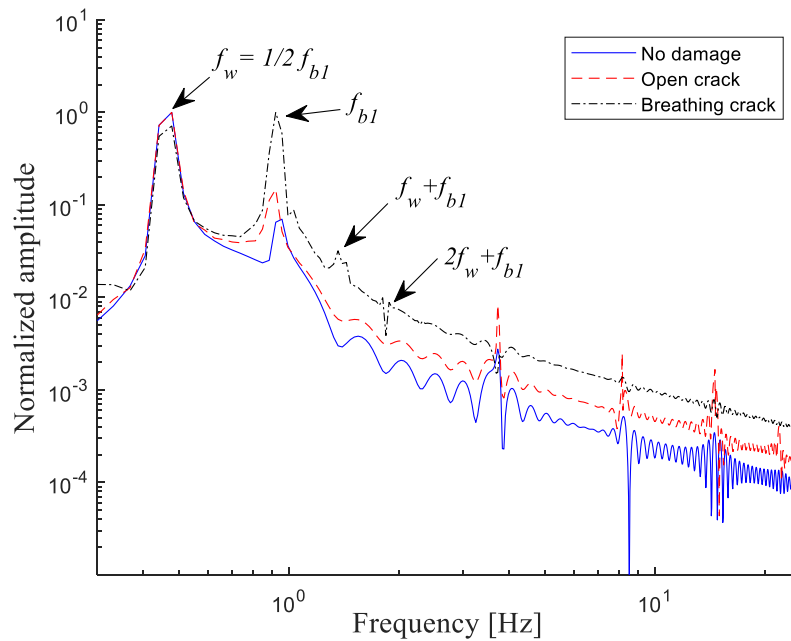
(a) For frequency of exciting force $f_w = 1/2\, f_{b1}$
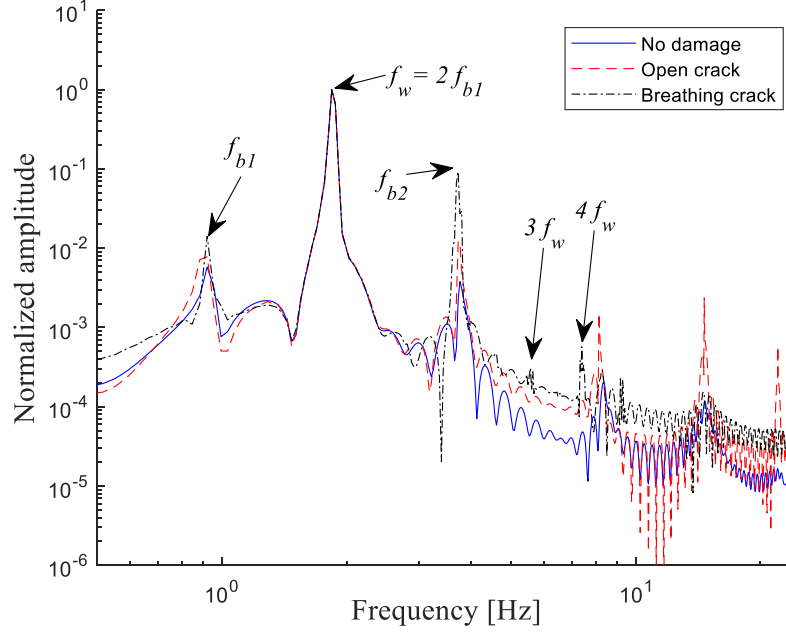
(b) For frequency of exciting force $f_w=2\,f_{b1}$

Figure 4 Spectra of bridge response considering different damage cases and exciting forces

4.3 Nonlinear characteristics of the cracked bridge under moving loads

The bridge acceleration response is analyzed to extract the nonlinear characteristics of the cracked bridge under moving loads using the proposed CSO-VMD. 5% Gaussian white noise is added to the acceleration response to simulate the measurement in the real situation. The setting of parameters for the CSO-VMD is: the total number of chickens $N=30$, the number of roosters N_r=round $(0.15*N)$, hens N_h= round $(0.7*N)$, chicks $N_c=(N-N_r-N_h)$ and mother hens N_m=round $(0.5*\,N_h)$, the maximum iterations $T_{max}=100$, and the frequency of change of hierarchical order $G=10$. The range of model number K is set as [2, 10] and the range of penalty factor α is set as [1000, 10000], respectively. The CSO-VMD is used to decompose the bridge response into mono-components. The component related to the first bridge dynamic mode is analyzed by ridge detection for IF identification since the first mode is usually the dominant mode of the considered bridge model.

The nonlinear characteristic of the bridge with single crack and multiple cracks under one moving load is first investigated. For the single crack scenario, the crack is at the mid-span of bridge, with crack depth ratio a/h=0.2 and 0.4, respectively. Figure 5(a) shows the identified IFs considering the open and breathing crack cases from responses at the mid-span. The figure shows that the identified IFs for open crack cases are approximately constant during the passage of the moving load and very close to the first bridge natural frequency. For the breathing crack cases, the IFs are time-varying that reach a minimum at the crack location. The location of the IF minimum values indicates the location of the breathing crack well. In this study, the nonlinear bridge dynamic behaviour is due to the presence of breathing crack. When the vehicular load is at the different locations on the bridge, the moment or curvature at the crack location is changed and that induces the crack opening and closing. The opening and closing of the crack would lead to the instantaneous change of the stiffness. Therefore, the IFs identified from the nonlinear bridge dynamic response are time-dependent that would change during the passage of the moving load along the bridge. Figure 5(b) shows a comparison of the instantaneous frequency for a/h= 0.4 extracted using ridge detection of the TFR and HT, respectively. The colors in Figure 5(b) represents the TFR amplitude of the extracted

component related to the first bridge dynamic mode. The results show that the IF from HT is modulated by a fast-varying component and it is hard to be extracted clearly. The proposed method can eliminate the fast-varying component of IF and the accurate nonlinear dynamic information of bridge can be obtained.

For two-crack case, the crack depth ratios and locations are set as: a/h=0.4 at $1/5L$ and a/h=0.3 at $3/5L$, respectively. The acceleration responses at $1/4L$ and $1/2L$ of the bridge under the moving load are analyzed. Figure 6 shows the identified IF results considering the breathing crack case. The results show that there are two local minimums in the IFs which are corresponding to the locations of two cracks (at 10m and 30m, respectively). The results identified from responses at different measurement points are very close expect at the two ends. The distortion at the ends of the instantaneous frequency curves is due to end effect of VMD caused by the finite duration of the measured signal. In VMD, due to the original signal is always non-periodic and finite length, recovering after the Hilbert transform and Fourier transform, there will be distortion at two ends. The end effect of modal decomposition can be reduced by the mutual information extension. It will be further study in the quantitative analysis for determining the damage extent, especially for the damage around the supports.
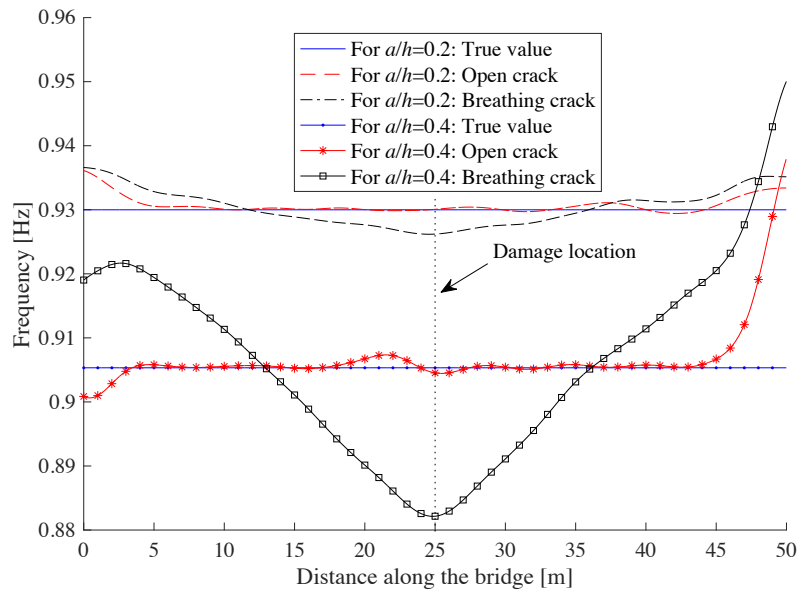
(a) IFs of bridge considering different crack cases
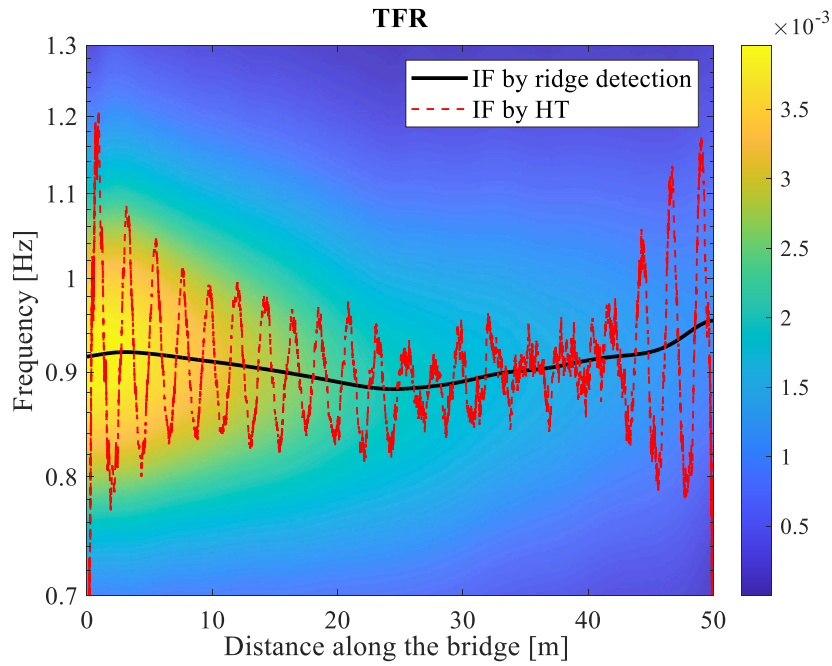
(b) IFs identified by ridge detection and HT

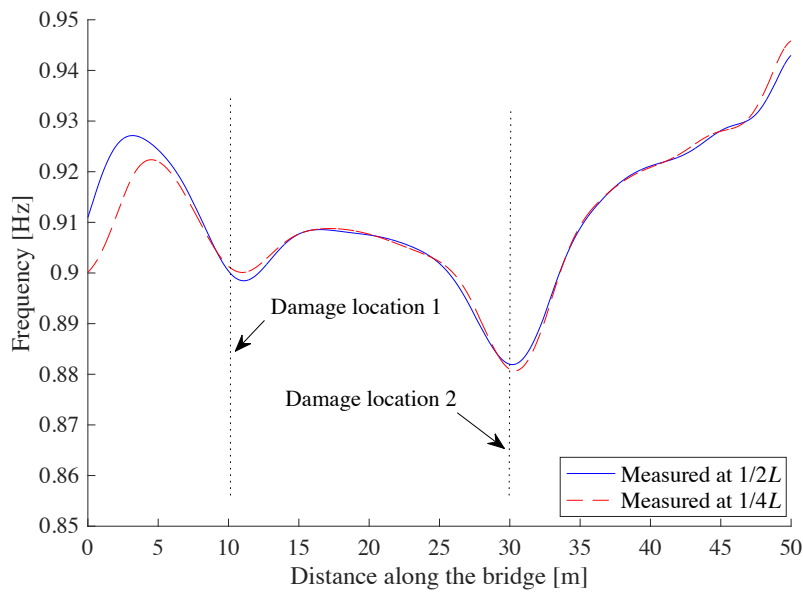Figure 5 IFs of bridge subjected to a moving load considering a single crack

Figure 6 IFs of bridge subject to a moving load considering multiple cracks

The nonlinear characteristic of bridge with multiple breathing cracks subjected to multiple moving loads is investigated. Two loads with a distance of 4.27m, where the front one is 40kN and the rear one is 60kN, move successively along the bridge with a speed of 2m/s. Figure 7(a) shows the IFs identified from the bridge mid-span acceleration. The results show that there are two minimum values of the IF during the passage of the loads on the bridge. The first minimum value is at about 15m and the other one is between 30m and 35m of the bridge. The distance in the x-axis of figures showing instantaneous frequency and instantaneous curvature denotes the moving distance of first (/front) load to the left support of the bridge. The results indicate that the IF reaches to a local minimum value at about the time when the second load arrives at the crack locations. Therefore, after shifting with the

distance between two loads, that is subtracting 4.27m from the locations of the minimum IF values in the figure, can improve the accuracy of crack localization under given conditions. Figure 7(b) shows the instantaneous curvatures of the bridge under moving loads. The maximum values of the instantaneous curvatures occur at crack locations, respectively. The results are consistent with the analytical model of the breathing crack in Section 2.2.2 that the maximum curvature leads to the full open of the breathing crack. The effect of measurement noise is also studied by considering another two levels of Gaussian noise to the response measurement, i.e., 10% and 15%, respectively. The results in Figure 7(a) show that the measurement noise has little effect on the identified IFs by the proposed method.
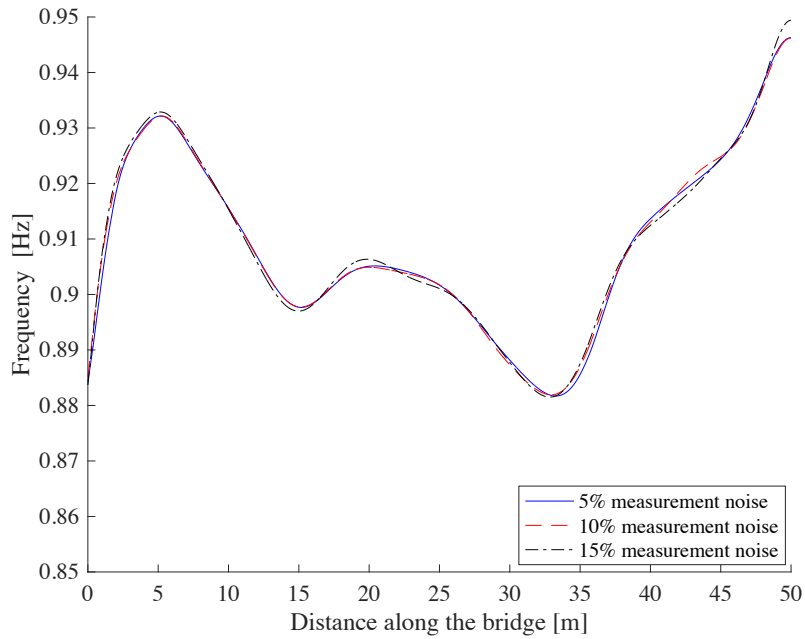
(a) Instantaneous frequencies
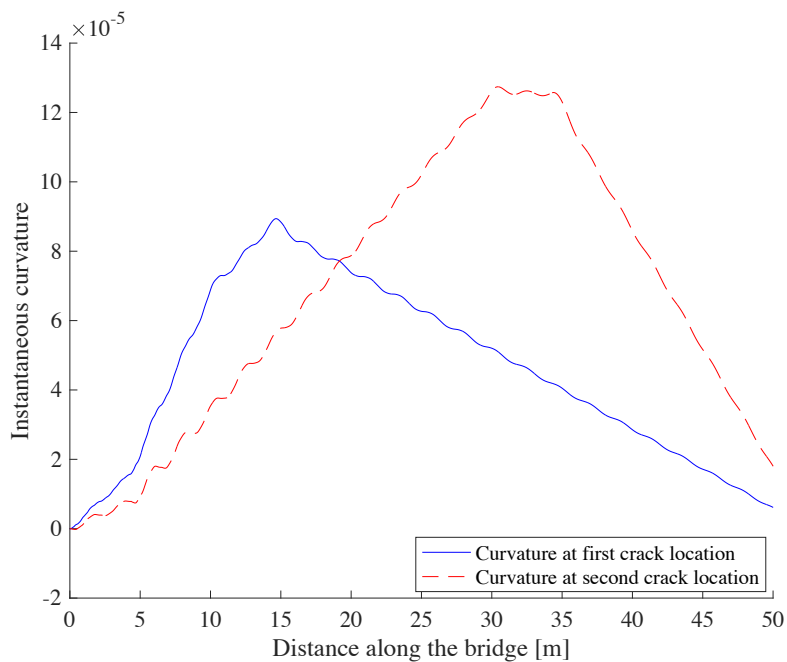
(b) Instantaneous curvatures at crack locations

Figure 7 Instantaneous frequencies and curvatures of bridge considering multiple loads and cracks

4.4 Nonlinear characteristics of cracked bridge considering VBI

In previous study, the constant moving load is considered. However, when heavy vehicle is passing over the bridge, the dynamic interaction between the vehicle and bridge needs to be considered. The nonstationary and nonlinear dynamic characteristics of cracked bridge due to the VBI needs further investigation. A widely used VBI model in the literature is considered as shown in Figure 8, where the vehicle is modeled as a two-axle half-car with 4 degrees-of-freedom. The motion equation of the VBI system considering a random road surface roughness can be found in [47]. The adopted vehicle parameters and dimensions are given in Table 1. The natural frequencies of the vehicle are 1.63, 2.30, 10.35 and 15.10Hz, respectively. The bridge acceleration response at midspan during the passing of the vehicle is measured. The speed of vehicle is 2m/s and 5% measurement noise is added.
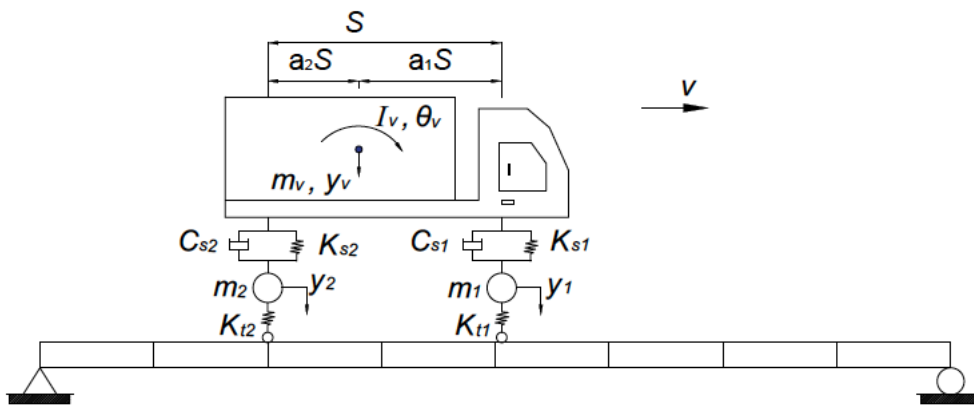
Figure 8 Vehicle-bridge interaction model

Table 1 Properties of the vehicle model

Property	Unit	Symbol	Value
Body mass	kg	m_v	17735
Pitch moment of inertia	kg m^2	I_v	147000
Mass of front axle	kg	m_1	1500
Mass of rear axle	kg	m_2	1000
Stiffness of front suspension	N/m	K_{s1}	2.47×10^6
Stiffness of rear suspension	N/m	K_{s2}	4.23×10^6
Damping of front suspension	N s/m	C_{s1}	3.00×10^4
Damping of rear suspension	N s/m	C_{s2}	4.00×10^4
Stiffness of front tyre	N/m	K_{t1}	3.74×10^6
Stiffness of rear tyre	N/m	K_{t2}	4.60×10^6
Axle distance	m	S	4.27
Axle distance ratio		a_1/a_2	0.52/0.48

4.4.1 Nonlinear characteristics of bridge for a smooth road surface

The IFs of bridge with a smooth road surface subjected to the moving vehicle are identified for open and breathing crack cases. Single crack and multi-crack conditions are the same as that in Section 4.3. Figure 9 shows the identified IFs for single crack situation. For both of the open and

breathing crack cases, the IFs are time-varying. The IFs decrease to a minimum around the midspan and then increase to form a variation trend of sinusoidal wave. This variation trend is due to the interaction between the vehicle and bridge which is consistent with the findings in the literature [48]. Comparing the results for open and breathing crack cases in Figure 9, the amplitude of IF variation at the crack location is enlarged for breathing crack case due to its opening when the vehicle arrives near the crack location at midspan. For the multi-crack scenario, the IFs and instantaneous curvatures of bridge at crack locations are shown in Figures 10(a) and 10(b), respectively. The results show that the local reduction of the IFs correspond to the maximum values of the instantaneous curvatures at crack locations which indicates the full open of the breathing cracks.
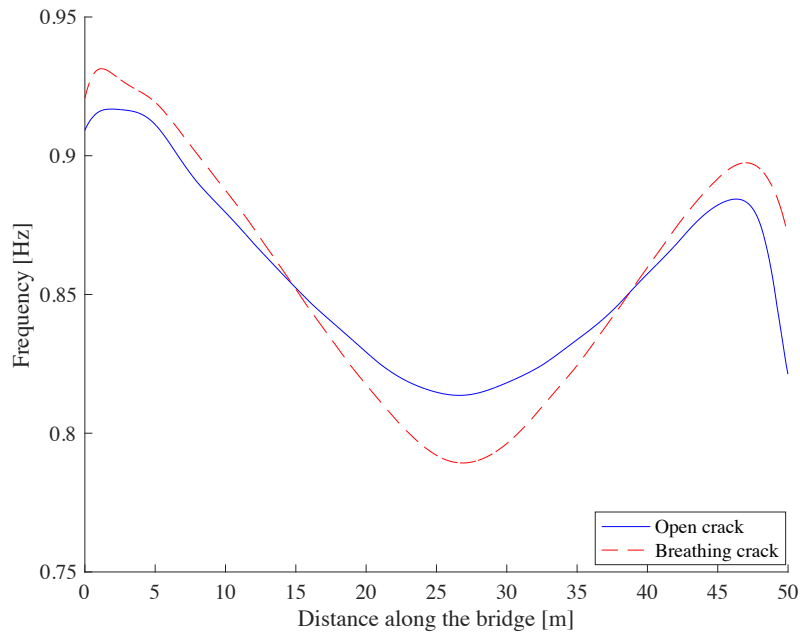
Figure 9 IFs of bridge subjected to a moving vehicle considering a single crack

(a) IFs

17
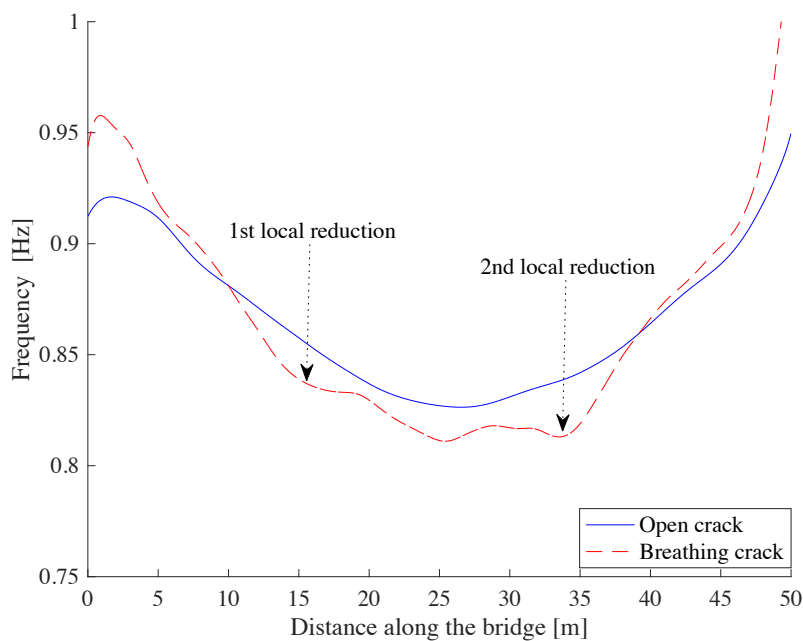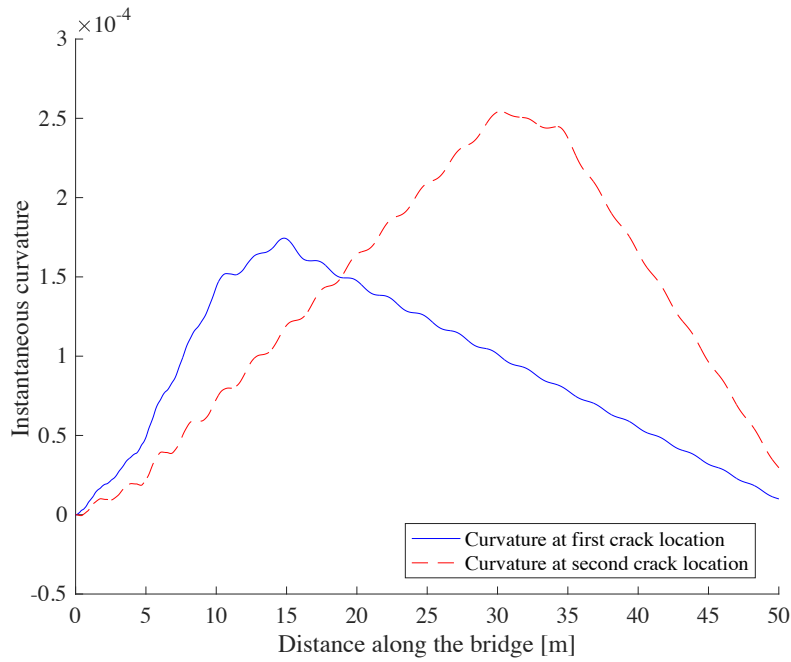
(b) Instantaneous curvatures at crack locations

Figure 10 IFs and curvatures of bridge subjected to a moving vehicle and multiple cracks

4.4.2 Nonlinear characteristics of bridge with a rough road surface

The nonlinear characteristics of bridge with the same single and multi-crack conditions are respectively considered except that a random road surface roughness is included. Figures 11 and 12 show the identified IFs of bridge under moving vehicle for single and multi-crack conditions, respectively. The results show that the IFs of bridge contain fluctuations due to the modulation of random roughness. It makes the localization of breathing crack difficult using the IF of breathing crack case alone. However, when compared to the bridge IF of open crack case, there is an obvious IF reduction at the midspan of the bridge for single crack condition, as shown in Figure 11. For the multi-crack condition, two obvious local IF reductions near the crack locations can also be observed, as shown in Figure 12. The reduction of IF values of breathing crack case compared to the open crack case is due to the open of breathing cracks for both conditions. Therefore, the identified nonlinear characteristics due to the breathing cracks of bridge can provide preliminary information to estimate the crack locations.
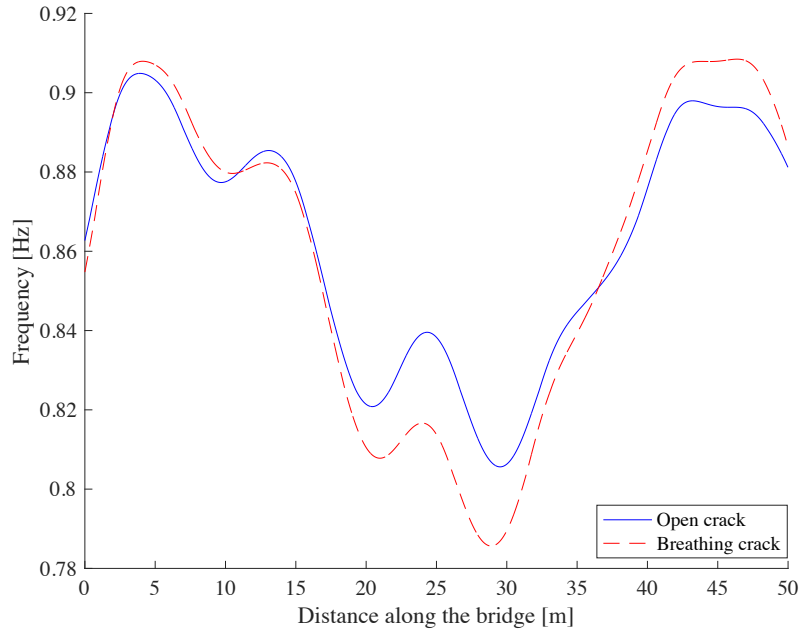
Figure 11 IFs of bridge subjected to a moving vehicle considering a single crack and roughness
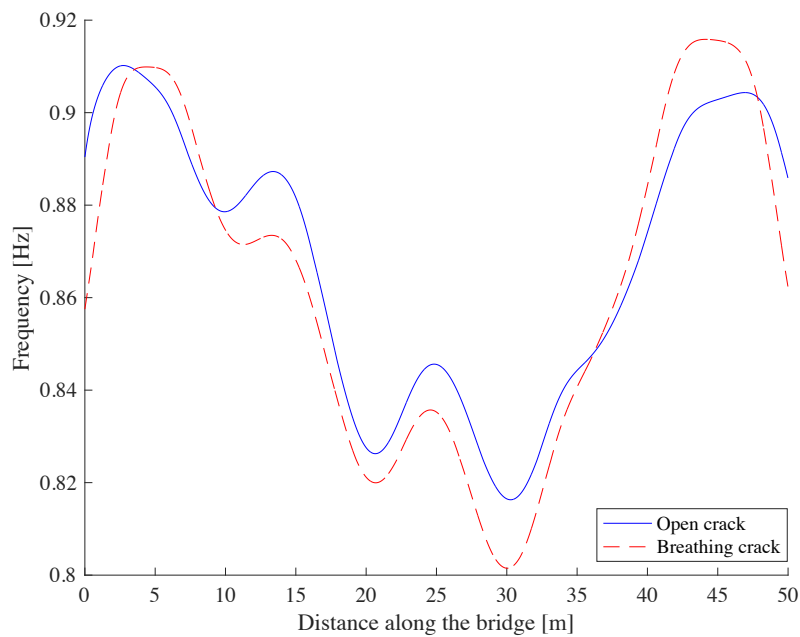

Figure 12 IFs of bridge subjected to a moving vehicle considering multiple cracks and roughness

4.5 Comparison of the proposed CSO-VMD to the conventional VMD

The superiority of the proposed CSO-VMD over the conventional VMD is demonstrated by examining their performance in bridge response decomposition. The bridge acceleration response when the vehicle moves over the rough bridge deck is analyzed. Figure 13 shows the bridge response and response spectrum considering aforementioned multiple breathing cracks. From the spectrum, it shows that the bridge response contains the dynamic components related to the vehicle due to VBI, indicated as f_{v1} and f_{v2} in the figure. The f_{b1} represents the first natural frequency of bridge. The parameter setting for the CSO-VMD is the same as the above. For the CSO-VMD, the identified

optimal number of modes in the response is 6 and the optimal penalty factor is 9850. For the conventional VMD, the mode number 6 is used, and penalty factor is 8373 (=0.85*9850) which are deliberately selected to close the optimal values. The decomposition performance of CSO-VMD and VMD is studied. Figures 14(a) and 14(b) show the extracted first four components in time and frequency domains, respectively. The fifth and sixth components are related to the higher modes of bridge and the results from two methods are very similar which are therefore not presented accordingly. The first component from two methods is the related to the first modal frequency of bridge. The second and third modes from CSO-VMD are related to the vehicle frequencies f_{v1} and f_{v2}, respectively. The results indicate that the CSO-VMD successfully extracts the slight component related to the vehicle dynamic mode f_{v1}, as shown in Figure 14(b). While, the second and third modes from conventional VMD are both related to f_{v2}. The components related to f_{v1} and f_{v2} are not well separated. The fourth mode is related to the third bridge dynamic mode. It can be seen that the CSO-VMD provides better decomposition performance than VMD due to the parameter optimization.
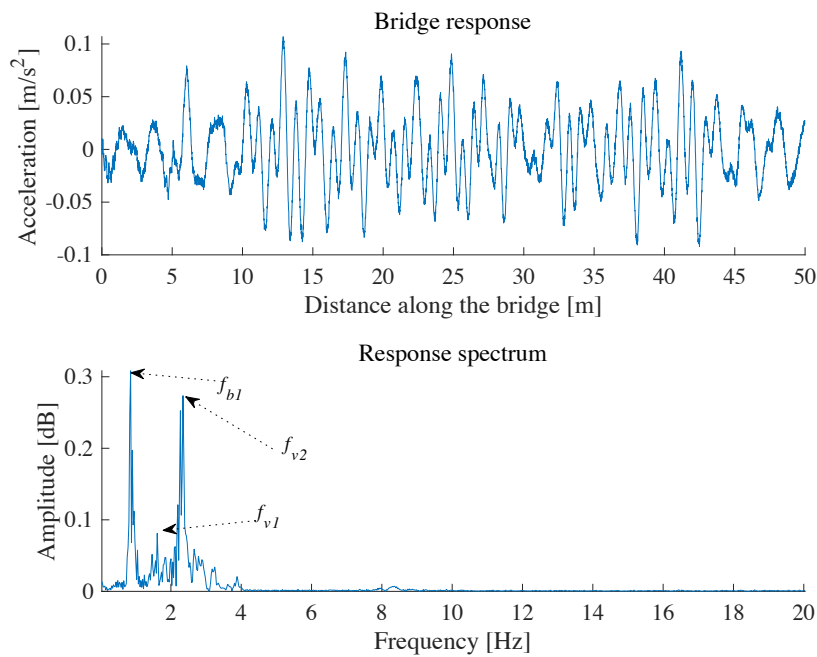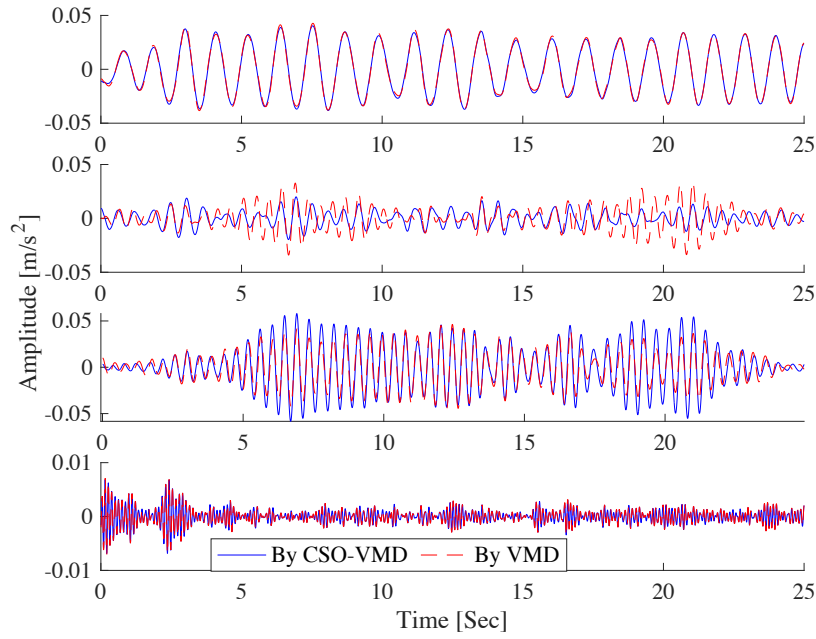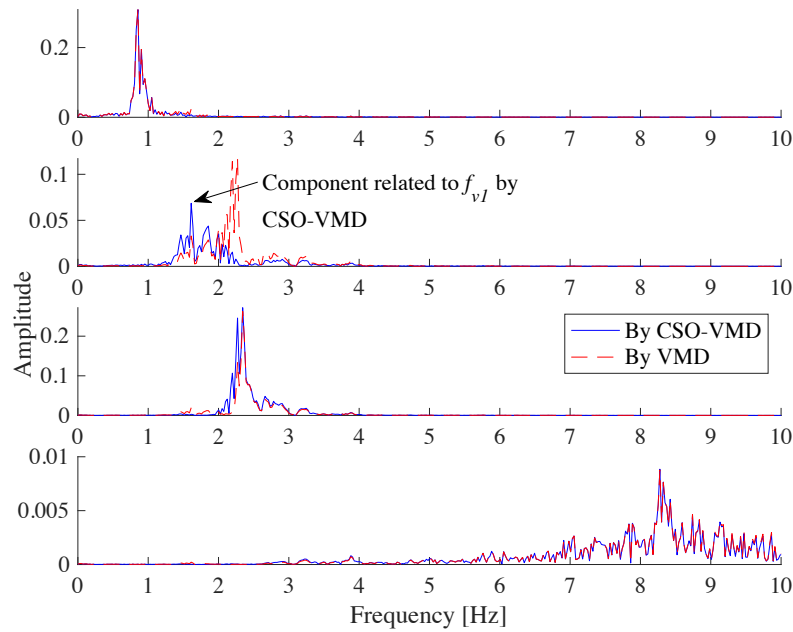

Figure 13 Bridge response and response spectrum

(a) Components in time domain

(b) Components in frequency domain

Figure 14 Bridge response decomposition by CSO-VMD and VMD

5. Laboratory experimental study

5.1 Experimental set-up and test procedures

Reinforced concrete Tee-section beam (RC Tee-beam) is a typical structural component to fabricate simply supported highway bridges. An experimental investigation on the dynamic characteristics of the RC Tee-beam is conducted. The schematic description of the experimental set-up is presented in Figure 15(a), which includes three Tee-section reinforced concrete beams and a test model vehicle pulled by an electric motor to move along the beam. Three beams consist of the leading and trailing beams with a length 4.5m each and a main beam in the middle. The length of the

main beam is 5m and the dimensions of the cross-section are shown in Figure 15(b). A 60mm diameter hole is left in the beam rib for post-tensioning of the beam after introducing damage to the beam. The total mass of the beam is 1050kg. For the model vehicle, the axle spacing is 0.8m, and the wheel spacing is 0.39m with a total weight of 10.60kN. The vehicle/bridge weight ratio is 1.03 that can be considered as the situation of a bridge under an extra heavy vehicle. The vehicle moves along the beam at an approximate speed of 0.5m/s during the moving VBI tests. Seven accelerometers are evenly distributed at the bottom and along the beam to measure the dynamic responses of the beam. An INV300 data acquisition system is used to collect the data with the sampling frequency 2024.292 Hz.

The beam is tested in three different states, i.e., intact state case, small damage case, and large damage case, respectively. The damage is created in the form of cracks using incremental static load tests. For small damage case, a three-point load system was applied at $1/3L$ from the left support of the main beam with the peak static load to 50kN. The loading and unloading procedures caused several tensile cracks with a crack zone of 760mm length around the loading point. For the large damage case, similar loading procedure to the small damage case was applied at $2/3L$ of the beam at first. Further loading was applied with a four-point load system at $1/3L$ and $2/3L$ with the final load 105kN to create a crack zone 2371mm length. During the static load test, the monitoring of the loads and strains revealed the nonlinear deformation behaviors of the beam due to the cracks of the concrete.
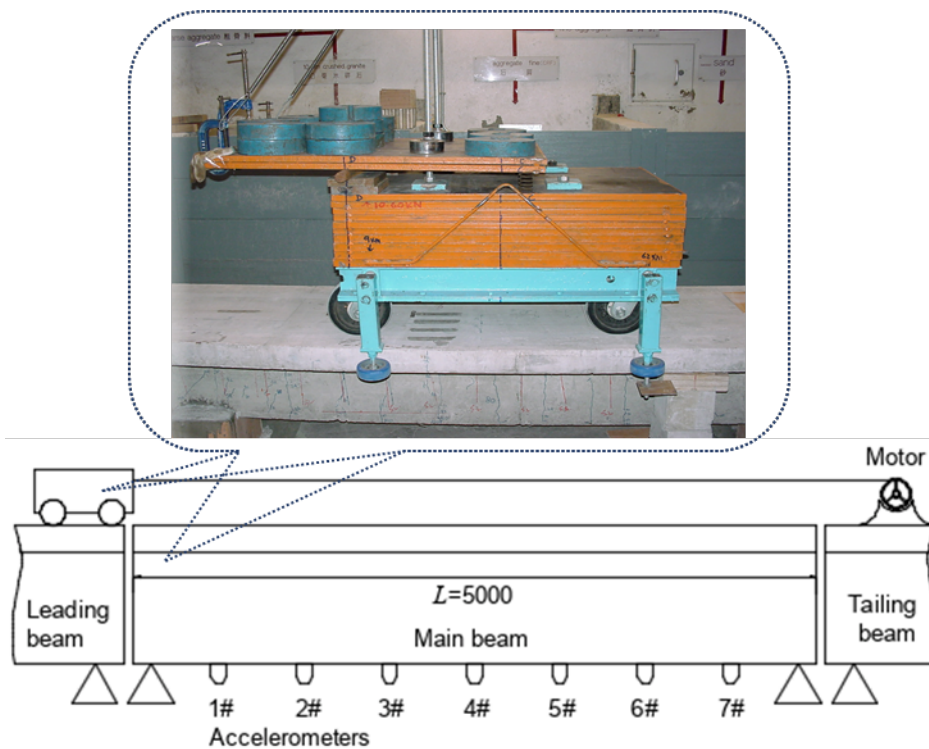
(a) Elevation view
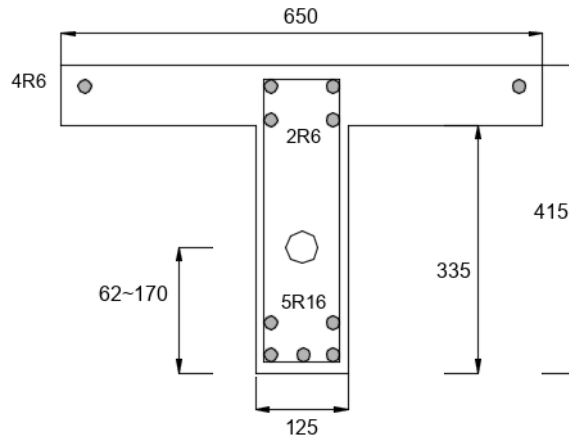
(b) Cross-section of the RC Tee-beam

Figure 15 Experimental set-up of the VBI test model

5.2 Experimental modal analysis

Impact hammer tests were performed with or without a 10.6kN static vehicle load in the middle of the main beam for the modal analysis of beam under different health cases. The identified natural frequencies for different cases are summarized in Table 2. When the vehicle is parked at the midspan, the first modal frequency is 16.04Hz that is close to the first vertical mode of the vehicle model 17.08Hz. The 2nd to 4th modes are corresponding to the first three modes of the beam when there is no static vehicle on top of the beam. When there is no damage, the first bridge modal frequency is 30.69Hz and 48.96Hz for the cases with and without static vehicle load, respectively. The frequency variation ratio due to the static vehicle load reaches 37.31% which is larger than those due to the damage. Moreover, the static vehicle load amplifies the difference in the natural frequencies between the undamaged and damaged cases because the load leads to the crack opening and the reduction of the flexural rigidity. The frequency change ratio between small damage case to large damage case is small compared to the change ratio between no damage case and damage case.

Table 2 Natural frequencies from modal analysis (unit: Hz)

Mode No.	Without static vehicle load			Mode No.	With static vehicle load		
	No damage	Small damage	Large damage		No damage	Small damage	Large damage
				1	16.04	12.51 (22.00%)	11.63 (27.49%)
1	30.69	27.02 (11.96%)	25.72 (16.19)	2	48.96	36.68 (25.08%)	34.23 (30.09%)
2	100.93	94.43 (6.44%)	88.84 (11.98)	3	104.45	97.52 (6.63%)	88.95 (14.84%)
3	168.25	158.39 (5.86%)	154.36 (8.26%)	4	180.22	178.15 (1.15%)	164.68 (8.62%)

Note: the percentage in parenthesis is the frequency change ratio to the 'No damage' case

The modal test results in Table 2 show that the presence of static vehicle on the bridge leads to an increase in the beam frequencies that means an increase of beam stiffness. It indicates that both the stiffness and mass of the vehicle contribute to the combined stiffness of the beam-vehicle system. This phenomenon has been found in a field test and it demonstrates that the effect of vehicle on the

bridge may cause distinguishable difference on the change of bridge modal frequencies [49]. In some extreme practical transportation situations, the weight of overloaded vehicle would be comparable to the weight of the bridge. It is important to investigate the non-stationary and non-linear dynamic characteristics of bridge due to the heavy vehicle load and structural cracks. Therefore, the experimental study fabricates the test VBI model that the weights of vehicle and bridge are comparable. This experimental modal test confirms the need to include the moving vehicles on top of the beam for an accurate dynamic analysis of the supporting beam.

5.3 Beam under moving vehicle

5.3.1 Spectrum analysis

Figure 16 shows the bridge responses at $1/2L$ and the power spectral densities of the responses under moving vehicle for different bridge conditions. The power spectral density is estimated via Burg's method with the length of window being 1024. In the spectra, two prominent peaks can be identified for each response. The first peak around 10Hz is related to the vehicle dynamic frequency, and the second peak is related to the first bridge frequency. The results show that the vehicle frequency remains the same for different bridge damage conditions, while there is a reduction in the bridge frequency when damage is introduced. Besides, the difference of identified bridge frequencies for small damage and large damage conditions is relatively small.
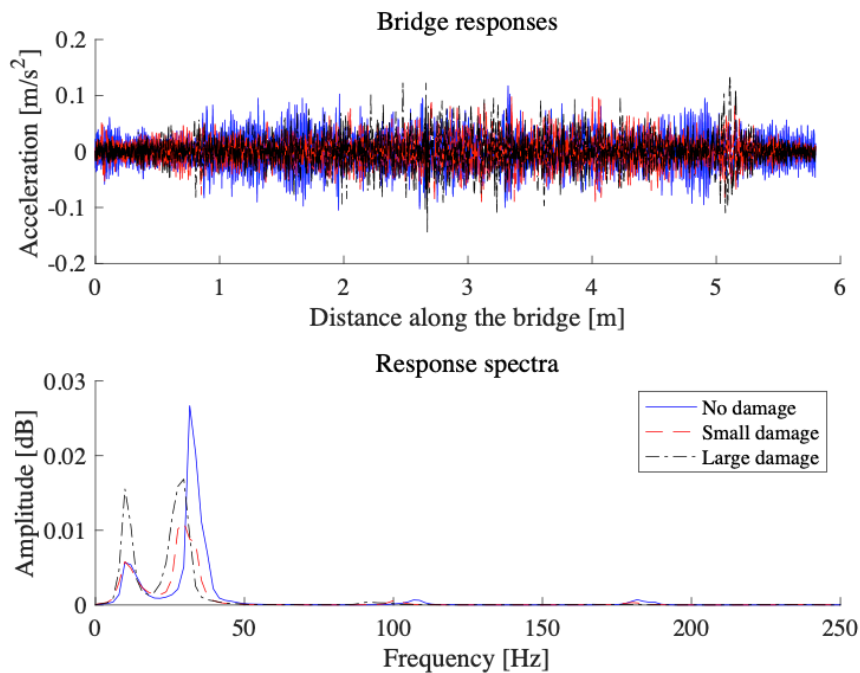

Figure 16 Bridge responses and spectra under moving vehicle load

5.3.2 Dynamic characteristics considering crack damages

The dynamic characteristics of beam under the moving vehicle load when the beam is no damage, with small damage, and with large damage are investigated. The identified IFs related to bridge dynamic responses measured at $3/8L$ of the beam are shown in Figure 17. It reveals critical dynamic characteristics of the beam in different damage states. In general, there is an increase in the IF due to the effect of moving vehicle load. The frequency reaches its maximum when the vehicle moves to the middle of the bridge span. When the same vehicle crosses the beam in small damage state and close to the first loading point, a net decrease in the frequency is observed due to the reduction of stiffness compared to the no damage case. When the vehicle passes the crack zone, the IF increases

to close to some part of the IF from no damage case around the midspan. After the large damage is introduced, the reduction in the IF is prominent for most of the time during the passage of the vehicle on the beam. When the IF for large damage case is compared to that of small damage case, it can be seen that the introduction of large damages at 2/3*L* of the main span causes local reduction of the IF after the passing of vehicle to the cracked zone. The acceleration responses measured from sensors at 1/8L, 4/8L, and 6/8L of the beam are used to analyze the sensitivity of the IF identification to the sensor location. Figure 18 shows the identified IFs from the responses measured at different locations for large damage state. The IF curves are generally in good agreement except some local difference around the two ends. The results demonstrate that the IF identification using proposed method is not sensitivity to the sensor location.

It is obvious that the IF curves of bridge under moving vehicle load are concave in the experimental study, while the IF curves in numerical study are mostly convex. The convex or concave of bridge IF curves depend on the vehicle/bridge frequency ratio that has been discussed in the literature [48]. When the bridge frequency is smaller than the vehicle frequency, the instantaneous frequency curve of the bridge will be convex and it will be concave if the bridge frequency is larger than the vehicle frequency. In the numerical study of this paper, the vehicle frequency is larger than the bridge frequency. The bridge frequency in experimental study is larger than the vehicle frequency.
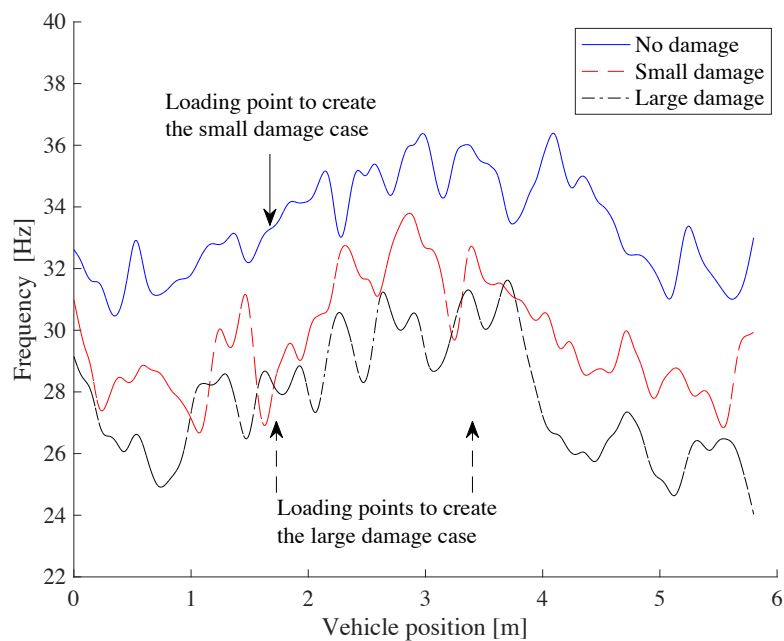

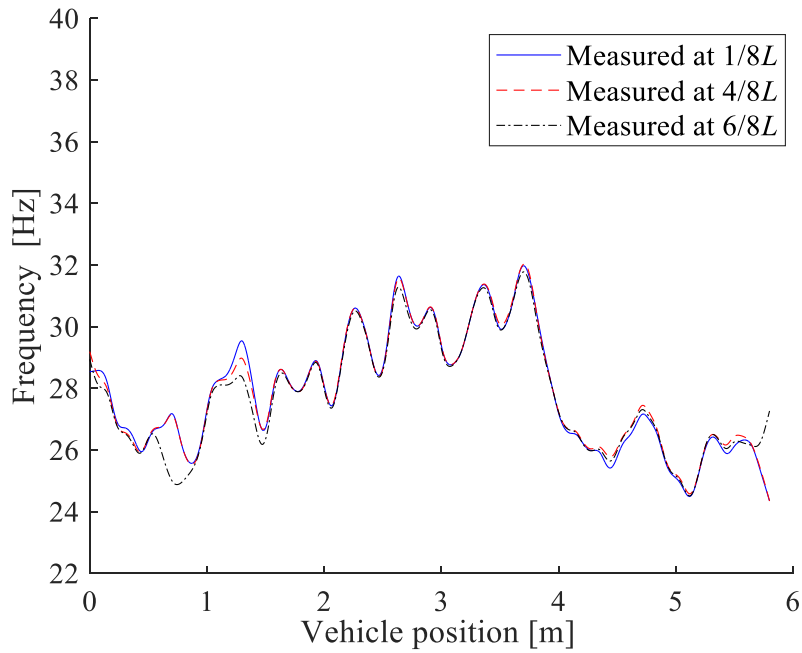Figure 17 The identified IFs considering different damage states

Figure 18 The identified IFs considering different measurement locations

5.3.3 Considering the effect of posttensioning

After the introduction of large damage to the beam and finishing previous tests, a 3*140kN tension force was applied to the cracked beam. Figure 19 shows the identified IF after posttensioning. The results show that the IF increases to a level that is close to that of no damage state. The results demonstrate that the stress leads to the regain of the stiffness loss due to the cracks.
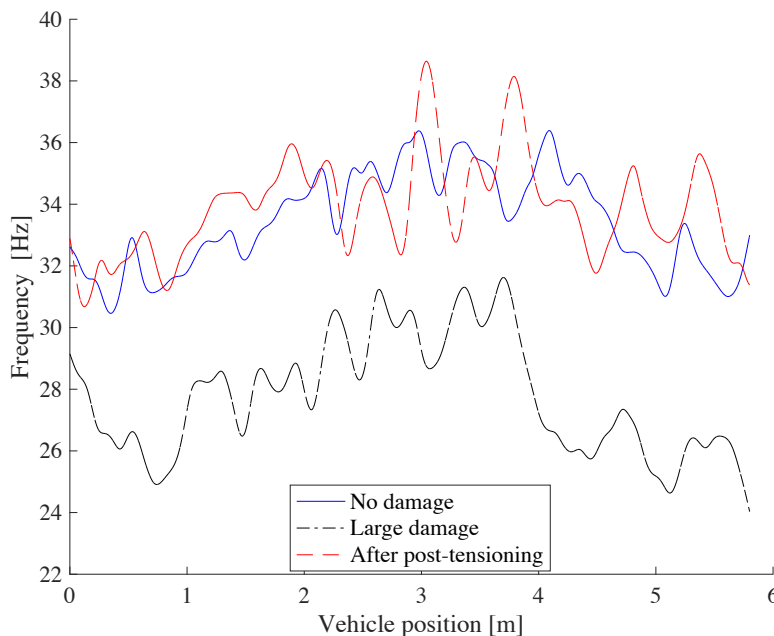

Figure 19 The identified IFs after posttensioning

6. Conclusions

The CSO-VMD with ridge detection has been developed to study the nonlinear characteristics of bridge subjected moving vehicle loads. The IF extracted from bridge related dynamic component

by the CSO-VMD is used to characterize the nonlinear behaviour of the damaged bridge. The parameter optimization for VMD by CSO improves the decomposition performance and the ridge detection for the IF extraction can avoid the interfere of the fast-varying frequency portion from HT. Numerical and experimental results have been used to verify the proposed method. Open and breathing crack models are introduced to simulate the damage on the bridge. The locations of the breathing cracks can be estimated using the extracted nonlinear dynamic characteristics. The effects of measurement noise, VBI and road surface roughness on the identified IFs have been discussed. The proposed method is much robust to the measurement noise. With the road surface roughness and VBI, the crack location can still be identified. Experimental study is further carried out on a RC T-beam under the moving model vehicle. Damage is created from incremental static loading in the form of cracks or crack zone. The identified IFs considering the combined effects of the moving vehicle and the damage reveal the nonstationary and nonlinear dynamic characteristics of the bridge. The increase of the IFs is observed due to the presence of the vehicle. The introduction of the cracks to the beam causes the general and localized reduction of IF which can be helpful for crack identification. Finally, the post-tensioning on the cracked beam is found to improve the beam stiffness significantly.

Reference

[1] Fan, W., and Qiao, P. (2011). Vibration-based damage identification methods: A review and comparative study. *Structural Health Monitoring*, 10(1), 83-111. https://doi.org/10.1177/1475921710365419

[2] Yang, Y.B., Wang, Z.L., Shi, K., Xu, H., and Wu, Y.T. (2020). State-of-the-art of vehicle-based methods for detecting various properties of highway bridges and railway tracks. *International Journal of Structural Stability and Dynamics*, 20(13), 2041004. https://doi.org/10.1142/S0219455420410047

[3] Han, W.S., Wu, J., Cai, C. S., and Chen, S.R. (2015). Characteristics and dynamic impact of overloaded extra heavy trucks on typical highway bridges. *Journal of Bridge Engineering*, 20(2), 05014011. http://dx.doi.org/10.1061/(ASCE)BE.1943-5592.0000666

[4] Sadeghi Eshkevari, S., Matarazzo, T. J., and Pakzad, S. N. (2020). Simplified vehicle–bridge interaction for medium to long-span bridges subject to random traffic load. *Journal of Civil Structural Health Monitoring*, 10(4), 693-707. https://doi.org/10.1007/s13349-020-00413-4

[5] Chang, K.C., Kim, C.W., and Borjigin, S. (2014). Variability in bridge frequency induced by a parked vehicle. *Smart Structures and Systems*, 13(5), 755-773. https://doi.org/10.12989/sss.2014.13.5.755

[6] Cantero, D., Hester, D., and Brownjohn, J. (2017). Evolution of bridge frequencies and modes of vibration during truck passage. *Engineering Structures*, 152, 452-64. https://doi.org/10.1016/j.engstruct.2017.09.039

[7] Borjigin, S., Kim, C.W., Chang, K.C., and Sugiura, K. (2018). Nonlinear dynamic response analysis of vehicle–bridge interactive system under strong earthquakes. *Engineering Structures*, 176, 500-521. https://doi.org/10.1016/j.engstruct.2018.09.014

[8] Neild, S.A., Williams, M.S., and McFadden, P.D. (2002). Non-linear behaviour of reinforced concrete beams under low-amplitude cyclic and vibration loads. *Engineering Structures*, 24(6), 707-718. https://doi.org/10.1016/S0141-0296(01)00134-1

[9] Andreaus, U., and Baragatti, P. (2011). Cracked beam identification by numerically analysing the nonlinear behaviour of the harmonically forced response. *Journal of Sound and Vibration, 330*(4), 721-742. https://doi.org/10.1016/j.jsv.2010.08.032

[10] Benfratello, S., Cacciola, P., Impollonia, N., Masnata, A., and Muscolino, G. (2007). Numerical and experimental verification of a technique for locating a fatigue crack on beams vibrating under Gaussian excitation. *Engineering Fracture Mechanics*, 74(18), 2992-3001. https://doi.org/10.1016/j.engfracmech.2006.06.023

[11] Bovsunovsky, A.P., and Surace, C. (2015). Non-linearities in the vibrations of elastic structures with a closing crack: A state of the art review. *Mechanical Systems and Signal Processing*, 62-63, 129-148. https://doi.org/10.1016/j.ymssp.2015.01.021

[12] Wei, C., and Shang, X. (2019). Analysis on nonlinear vibration of breathing cracked beam. *Journal of Sound and Vibration*, 461, 114901. https://doi.org/10.1016/j.jsv.2019.114901

[13] Mahmoud, M. A., and Abou Zaid, M. A. (2002). Dynamic response of a beam with a crack subject to a moving mass. *Journal of Sound and Vibration*, 256(4), 591-603. https://doi.org/10.1006/jsvi.2001.4213

[14] Ariaei, A., Ziaei-Rad, S., and Ghayour, M. (2009). Vibration analysis of beams with open and breathing cracks subjected to moving masses. *Journal of Sound and Vibration*, 326(3-5), 709-724. https://doi.org/10.1016/j.jsv.2009.05.013

[15] Law, S.S., and Zhu, X.Q. (2004). Dynamic behavior of damaged concrete bridge structures under moving vehicular loads. *Engineering Structures*, 26(9), 1279-93. https://doi.org/10.1016/j.engstruct.2004.04.007

[16] Abdel Wahab, M.M., De Roeck, G., and Peeters, B. (1999). Parameterization of damage in reinforced concrete structures using model updating. *Journal of Sound and Vibration*, 228(4), 717–30. https://doi.org/10.1006/jsvi.1999.2448

[17] Lee, J.H., and Fenves, G.L. (1998). Plastic-damage model for cyclic loading of concrete structures. *Journal of Engineering Mechanics*, 124(8), 892-900. https://doi.org/10.1061/(ASCE)0733-9399(1998)124:8(892)

[18] Nguyen, K. V. (2013). Comparison studies of open and breathing crack detections of a beam-like bridge subjected to a moving vehicle. *Engineering Structures*, 51, 306-314. https://doi.org/10.1016/j.engstruct.2013.01.018

[19] Yin, X.F., Liu, Y., Deng, L., and Kong, X. (2017). Dynamic behavior of damaged bridge with multi-cracks under moving vehicular loads. *International Journal of Structural Stability and Dynamics*, 17(02), 1750019. https://doi.org/10.1142/S0219455417500195

[20] Dimarogonas, A. D. (1996). Vibration of cracked structures: A state of the art review. *Engineering Fracture Mechanics*, 55(5), 831-857. https://doi.org/10.1016/0013-7944(94)00175-8

[21] Pakrashi, V., O'Connor, A., Basu, B. (2010). A bridge-vehicle interaction based experimental investigation of damage evolution. *Structural Health Monitoring*, 9(4), 285–296. https://doi.org/10.1177/1475921709352147

[22] McGetrick, P.J., and Kim, C.W. (2013). A parametric study of a drive by bridge inspection system based on the Morlet wavelet. *Key Engineering Materials*, 569-570, 262-269. https://doi.org/10.4028/www.scientific.net/KEM.569-570.262

[23] Mei, Q.P., Gül, M., and Boay, M. (2019). Indirect health monitoring of bridges using Mel-frequency cepstral coefficients and principal component analysis. *Mechanical Systems and Signal Processing*, 119, 523-546. https://doi.org/10.1016/j.ymssp.2018.10.006

[24] Cantero, D., McGetrick, P., Kim, C.W., and O'Brien, E. (2019). Experimental monitoring of bridge frequency evolution during the passage of vehicles with different suspension properties. *Engineering Structures,* 187, 209-219. https://doi.org/10.1016/j.engstruct.2019.02.065

[25] Wang, H.Q., Nagayama, T., Nakasuka, J., Zhao, B.Y., and Su, D. (2018). Extraction of bridge fundamental frequency from estimated vehicle excitation through a particle filter approach. *Journal of Sound and Vibration*, 428, 44-58. https://doi.org/10.1016/j.jsv.2018.04.030

[26] Zhan, J.W., Zhang, F., Siahkouhi, M., Kong, X., and Xia, H. (2021). A damage identification method for connections of adjacent box-beam bridges using vehicle-bridge interaction analysis and model updating. *Engineering Structures*, 228, 111551. https://doi.org/10.1016/j.engstruct.2020.111551

[27] Kildashti, K., Makki Alamdari, M., Kim, C.W., Gao, W., and Samali, B. (2020). Drive-by-bridge inspection for damage identification in a cable-stayed bridge: Numerical investigations. *Engineering Structures*, 223, 110891. https://doi.org/10.1016/j.engstruct.2020.110891

[28] Li, J.T., Guo, J., and Zhu, X.Q. (2021). Time-varying parameter identification of bridges subject to moving vehicles using ridge extraction based on empirical wavelet transform. *International Journal of Structural Stability and Dynamics*, 21(04), 2150046. https://doi.org/10.1142/S0219455421500462

[29] Zhang, J., Yang, D., Ren, W.X., and Yuan, Y. (2021). Time-varying characteristics analysis of vehicle-bridge interaction system based on modified S-transform reassignment technique. *Mechanical Systems and Signal Processing*, 160, 107807. https://doi.org/10.1016/j.ymssp.2021.107807

[30] Dragomiretskiy, K., and Zosso, D. (2014). Variational Mode Decomposition. *IEEE Transactions on Signal Processing*, 62, 531-544. https://doi.org/10.1109/TSP.2013.2288675

[31] Xin, Y., Li, J., and Hao, H. (2020). Damage detection in initially nonlinear structures based on variational mode decomposition. *International Journal of Structural Stability and Dynamics*, 20(10), 2042009. https://doi.org/10.1142/S0219455420420092

[32] Tian, Y.D., and Zhang, J. (2020). Structural flexibility identification via moving-vehicle-induced time-varying modal parameters. *Journal of Sound and Vibration*, 474, 115264. https://doi.org/10.1016/j.jsv.2020.115264

[33] Yang, Y.B., Shi, K., Wang, Z.L., Xu, H., Zhang, B., and Wu, Y.T. (2021). Using a single-DOF test vehicle to simultaneously retrieve the first few frequencies and damping ratios of the bridge. *International Journal of Structural Stability and Dynamics*, 21(08), 2150108. https://doi.org/10.1142/S021945542150108X

[34] Li, H., Liu, T., Wu, X., and Chen, Q. (2020). An optimized VMD method and its applications in bearing fault diagnosis. *Measurement*, 166, 108185. https://doi.org/10.1016/j.measurement.2020.108185

[35] Meng, X. B., Liu, Y., Gao, X. Z., and Zhang, H. Z. (2014). A new bio-inspired algorithm: chicken swarm optimization. *International Conference in Swarm Intelligence*, Springer, 86-94. https://doi.org/10.1007/978-3-319-11857-4_10

[36] Li, Y. T., Wu, Y., and Qu, X. J. (2017). Chicken swarm-based method for ascent trajectory optimization of hypersonic vehicles. *Journal of Aerospace Engineering*, 30(5), 04017043, 1-12. https://doi.org/10.1061/(ASCE)AS.1943-5525.0000757

[37] Deb, S., Gao, X. Z., Tammi, K., Kalita, K., and Mahanta, P. (2020). Recent Studies on Chicken Swarm Optimization algorithm: a review (2014–2018). *Artificial Intelligence Review*, 53(3), 1737-1765. https://doi.org/10.1007/s10462-019-09718-3

[38] Zheng, D.Y., and Kessissoglou, N.J. (2002). Free vibration analysis of a cracked beam by finite element method. *Journal of Sound and Vibration*, 273, 457-475. https://doi.org/10.1016/S0022-460X(03)00504-2

[39] Bertsekas, D. P. (1982). Constrained optimization and Lagrange Multiplier methods. *Computer Science and Applied Mathematics*, Academic Press, Boston. https://doi.org/10.1016/C2013-0-10366-2

[40] Huang, Q. Y., Liu, X., Li, Q., Zhou, Y., Yang, T., and Ran, M. X. (2021). A parameter-optimized variational mode decomposition method using salp swarm algorithm and its application to acoustic-based detection for internal defects of arc magnets. *AIP Advances*, 11(6), 065216. http://dx.doi.org/10.1063/5.0054894

[41] Wang, Z.C., Xin, Y., and Ren, W.X. (2015). Nonlinear structural model updating based on instantaneous frequencies and amplitudes of the decomposed dynamic responses. *Engineering Structures*, 100, 189-200. https://doi.org/10.1016/j.engstruct.2015.06.002

[42] Iatsenko, D., McClintock, P .V. E., and Stefanovska, A. (2016). Extraction of instantaneous frequencies from ridges in time-frequency representations of signals. *Signal Processing*, 125: 290-303. https://doi.org/10.1016/j.sigpro.2016.01.024

[43] Sinha, J.K. (2009). Higher order coherences for fatigue crack detection. *Engineering Structures*, 31(2), 534-538. https://doi.org/10.1016/j.engstruct.2008.10.004

[44] Long, H., Liu, Y.L., and Liu, K.F. (2019). Nonlinear vibration analysis of a beam with a breathing crack. *Applied Sciences*, 9(18), 3874. https://doi.org/10.3390/app9183874

[45] Bovsunovsky, A.P., Surace, C., and Bovsunovsky, O.A. (2006). The effect of damping and force application point on the non-linear dynamic behaviour of a cracked beam at sub and superresonance vibrations. Strength of Materials, 38(5), 492-497. https://doi.org/10.1007/s11223-006-0068-8

[46] Pugno, N., Surace, C., and Ruotolo, R. (2000). Evaluation of the non-linear dynamic response to harmonic excitation of a beam with several breathing cracks. *Journal of Sound and Vibration*, 235(5), 749-762. https://doi.org/10.1006/jsvi.2000.2980

[47] Li, J. T., Zhu, X. Q., Law, S. S., and Samali, B. (2020). A two-step drive-by bridge damage detection using dual Kalman filter. *International Journal of Structural Stability and Dynamics*, 20(10), 2042006. https://doi.org/10.1142/S0219455420420067

[48] Yang, Y.B., Cheng, M.C., and Chang, K.C. (2013). Frequency variation in vehicle–bridge interaction systems. *International Journal of Structural Stability and Dynamics*, 13(02), 1350019. https://doi.org/10.1142/S0219455413500193

[49] Kim, C.Y., Jung, D.S., Kim, N.S., Kwon, S.D., and Feng, M.Q. (2003). Effect of vehicle weight on natural frequencies of bridges measured from traffic-induced vibration. *Earthquake Engineering and Engineering Vibration*, 2(1), 109-115. https://doi.org/10.1007/BF02857543